R-1509

AD 742455

DAVIDSON LABORATORY

Report SIT-DL-72-1509
February 1972

AN EXACT LINEAR LIFTING-SURFACE THEORY FOR A MARINE PROPELLER IN A NONUNIFORM FLOW FIELD

DDC
MAY 30 1972
A

by

S. Tsakonas
W.R. Jacobs
M.R. Ali

This Research was Sponsored by the Naval Ship Research and Development Center, General Hydromechanics Research Program Under Contract N00014-67-A-0202-0018

Reproduced by
NATIONAL TECHNICAL INFORMATION SERVICE
Springfield Va 22151

APPROVED FOR PUBLIC RELEASE
DISTRIBUTION UNLIMITED

STEVENS INSTITUTE OF TECHNOLOGY
CASTLE POINT STATION
HOBOKEN NEW JERSEY 07030

55

UNCLASSIFIED
Security Classification

DOCUMENT CONTROL DATA - R & D

(Security classification of title, body of abstract and indexing annotation must be entered when the overall report is classified)

1. ORIGINATING ACTIVITY (Corporate author) DAVIDSON LABORATORY, STEVENS INSTITUTE OF TECHNOLOGY	2a. REPORT SECURITY CLASSIFICATION UNCLASSIFIED 2b. GROUP

3. REPORT TITLE

AN EXACT LINEAR LIFTING-SURFACE THEORY FOR A MARINE PROPELLER IN A NONUNIFORM FLOW FIELD.

4. DESCRIPTIVE NOTES (Type of report and inclusive dates)

FINAL

5. AUTHOR(S) (First name, middle initial, last name)

S. TSAKONAS, W.R. JACOBS AND M.R. ALI.

6. REPORT DATE FEBRUARY 1972	7a. TOTAL NO. OF PAGES 50	7b. NO. OF REFS 12
8a. CONTRACT OR GRANT NO. N00014-67-A-0202-0018 b. PROJECT NO. c. d.	9a. ORIGINATOR'S REPORT NUMBER(S) SIT-DL-72-1509 9b. OTHER REPORT NO(S) (Any other numbers that may be assigned this report)	

10. DISTRIBUTION STATEMENT

APPROVED FOR PUBLIC RELEASE: DISTRIBUTION UNLIMITED.

11. SUPPLEMENTARY NOTES	12. SPONSORING MILITARY ACTIVITY NAVAL SHIP RESEARCH & DEVELOPMENT CENTER BETHESDA MARYLAND 20034

13. ABSTRACT

The mathematical model used in previous Davidson Laboratory adaptations of linearized unsteady lifting surface theory to marine propellers has been revised by removing the so-called "staircase" approximation of the blade wake and replacing it by an "exact" helicoidal blade wake. A new numerical procedure and program based on the present model has been developed to evaluate the steady and unsteady blade loading distributions, which are used to determine the bearing forces and moments. Systematic calculations of these forces and moments for a series of propellers show better agreement on the whole with experimental measurements than did the earlier calculations for the same series. In addition, the chordwise loading distributions are much smoother than obtained previously. However, the quantitative improvement must be weighed against the considerable increase in computer time over the old method.

DD FORM 1 NOV 65 1473 (PAGE 1)

S/N 0101-807-6811

UNCLASSIFIED
Security Classification

A-31408

UNCLASSIFIED
Security Classification

14. KEY WORDS	LINK A ROLE	LINK A WT	LINK B ROLE	LINK B WT	LINK C ROLE	LINK C WT
HYDRODYNAMICS						
UNSTEADY THEORY FOR MARINE PROPELLERS						

DD FORM 1 NOV 65 1473 (BACK)
S/N 0101-807-6821

UNCLASSIFIED
Security Classification

A-31409

DAVIDSON LABORATORY
Stevens Institute of Technology
Castle Point Station
Hoboken, New Jersey 07030

Report SIT-DL-72-1509

February 1972

AN EXACT LINEAR LIFTING-SURFACE THEORY FOR A MARINE PROPELLER IN A NONUNIFORM FLOW FIELD

by

S. Tsakonas

W.R. Jacobs

M.R. Ali

This Research was Sponsored by the Naval Ship Research and Development Center, General Hydromechanics Research Program under Contract N00014-67-A-0202-0018. [DL Project 3666/113.]

APPROVED FOR PUBLIC RELEASE: DISTRIBUTION UNLIMITED

Approved

J. P. Breslin, Director

26 pages + x
7 figures
4 appendices (14 pages)

ABSTRACT

The mathematical model used in previous Davidson Laboratory adaptations of linearized unsteady lifting surface theory to marine propellers has been revised by removing the so-called "staircase" approximation of the blade wake and replacing it by an "exact" helicoidal blade wake. A new numerical procedure and program based on the present model has been developed to evaluate the steady and unsteady blade loading distributions, which are used to determine the bearing forces and moments. Systematic calculations of these forces and moments for a series of propellers show better agreement on the whole with experimental measurements than did the earlier calculations for the same series. In addition, the chordwise loading distributions are much smoother than obtained previously. However, the quantitative improvement must be weighed against the considerable increase in computer time over the old method.

Keywords

Hydrodynamics

Unsteady Theory for Marine Propellers

TABLE OF CONTENTS

	Page
ABSTRACT	iii
NOMENCLATURE	vii
INTRODUCTION	1
LINEARIZED UNSTEADY LIFTING-SURFACE THEORY	3
DEVELOPMENT OF THE KERNEL FUNCTION	4
REDUCTION TO A ONE-DIMENSIONAL INTEGRAL EQUATION	10
PROPELLER LOADING AND RESULTING FORCES AND MOMENTS	15
Loading	16
Propeller-Generated Forces and Moments	16
Blade Bending Moments	17
NUMERICAL RESULTS	18
CONCLUSIONS	23
REFERENCES	25

FIGURES

APPENDIX A: Singularity of the Kernel Function at $\rho = r$

APPENDIX B: Evaluation of the θ_α- and φ_α-integrals

APPENDIX C: Evaluation of the Integrand of the λ-integral at the Singularity $\lambda = 0$

APPENDIX D: Evaluation by the Lagrange Interpolation Method of the ρ-integration in the Region of the Singularity

NOMENCLATURE

a	Ω/U
$B_{\bar{m},\bar{n}}(\lambda)$	function defined in Eq. (28)
$b(r)$	expanded semichord length at each radius, ft
$F_{x,y,z}$	propeller-induced forces in x,y,z direction
$f(r,s)$	camberline ordinates from face pitch line at each radial position
$g(\lambda)$	function defined in Eq. (28)
$I_m(\ )$	modified Bessel function of first kind, or order m
$I^{(\bar{m})}(\ )$	defined in Appendix B
$I_1^{(\bar{m})}(\ )$	defined in Appendix B
$(IK)_m$	defined in Eq. (28)
i	index
$J_m(\ )$	Bessel function of order m
K	kernel of integral equation
$\bar{K}^{(\bar{m},\bar{n})}$	kernel after chordwise integrations
$K_m(\ )$	modified Bessel function of second kind, of order m
k	variable of integration
$k^{(m,\bar{n})}$	influence functions (Eq. 40)
L'	loading distribution in lb/ft^2
$L(r)$	spanwise loading distribution in lb/ft
$L^{(q,\bar{n})}(\rho)$	spanwise loading coefficients of Birnbaum distribution
ℓ	integer multiple
M_b	blade bending moment about face pitch line

$M_{\bar{r}}$	final value of m in summation
m	index of summation
$\bar{m}$	order of lift operator
N	number of blades
n	blade index
$\bar{n}$	order of chordwise mode
$\vec{n}$	normal to surface at loading point
$\vec{n}'$	normal to surface at control point
P	pressure
P(r)	pitch at each radial position
$Q_{x,y,z}$	propeller-induced moments about x,y,z axis
q	order of harmonic of inflow field
R', R	Descartes distance
r	radial ordinate of control point
r_o	propeller radius
S	propeller lifting surface
$S_{\bar{n}}$	normal sum of curtailed Birnbaum series
s	chordwise location as fraction of chord length
t	time, sec
U	uniform velocity
$V^{(q)}(r)$	Fourier coefficients of velocity distribution
$\bar{V}_c$	velocity due to camber effects
$\bar{V}_f$	velocity due to flow-incidence angles
W	velocity distribution normal to propeller
x	longitudinal ordinate of control point
x,r,φ	cylindrical coordinate system of control point

y	transverse cartesian ordinate
z	vertical cartesian ordinate
β	angle in Eq. (18)
β	half-length of radial strip
δ	small length
$\theta(\bar{n})$	chordwise modes (Eq. 21)
θ	angular ordinate of loading point
θ_o	angular position of loading point with respect to mid-chord line
θ_b	projected blade chordwise length, radians
$\bar{\theta}_n$	$\frac{2\pi}{N}(n-1)$, $n = 1, 2, \ldots N$
$\theta_p(r)$	geometric pitch angle at each radial position
θ_α	angular chordwise location of loading point
$\Lambda^{(\bar{n})}(x)$	defined in Appendix B
$\Lambda_1^{(\bar{n})}(x)$	defined in Appendix B
λ	order of harmonic of loading distribution
λ	variable of integration
ξ	longitudinal ordinate of loading point
ξ, ρ, θ	cylindrical coordinate system of loading point
ρ	radial ordinate of loading point
ρ_f	mass density of fluid
σ	angular measure of skewness
$\Delta\sigma$	$\sigma^r - \sigma^\rho$
$\sigma_{\bar{n}}$	Cesaro sum of curtailed Birnbaum series
τ'	variable of integration

Φ	velocity potential
$\Phi(\bar{m})$	generalized lift operator (Eq. 25)
φ	angular ordinate of control point
φ_o	angular position of control point with respect to midchord line
φ_α	angular chordwise location of control point
Ψ	acceleration potential
Ω	angular velocity of propeller
ω	angular frequency of loading

Superscripts

r	refers to control point
p	refers to control point

INTRODUCTION

In the course of a series of investigations concerned with adapting linearized unsteady lifting surface theory to marine propellers, Davidson Laboratory has sought to improve the mathematical model and techniques for solving the surface integral equation, and evaluating the propeller loading distributions and resulting hydrodynamic forces and moments (see for example Refs. 1-5). A new method[5] has been developed for the inversion of the downwash integral equation which employs the "generalized lift-operator" technique. This new approach eliminates many of the numerical difficulties arising in the commonly used "mode-collocation" method.

Certain mathematical simplifications have been introduced in these studies, in addition to those imposed by the linearized version of the problem. The major simplification is the approximation of the helicoidal propeller wake by a "staircase" function.[2] In Reference 1, which presents the exact treatment of the helicoidal wake for a simple sector-form blade with flat-plate chordwise loading distribution, the results are found to agree well with those for the same propeller computed with the staircase approximation of the wake. Admittedly, only one set of calculations was performed, under several conditions; the complications in the exact wake treatment considerably lengthened the computation time on a high-speed computer (IBM7090) and appeared too formidable to allow utilizing that method more fully at that time. It was felt that use of the exact treatment should be deferred until a time when more accurate experimental techniques would be established for measuring the hull wake upon which all calculations depend, thus justifying greater accuracy in the theoretical treatment.

In the meantime, the numerical procedure in the solution of the integral equation was being improved, a) by increasing the number of chordwise modes, b) by introducing more appropriate numerical schemes to deal with the singular behavior of the kernel function, with the problem of truncation of infinite series, and with the problem of "overlapping" of the wake generated by wide blades, and c) by accommodating arbitrary

blade camber variation. In addition, the problem of instability of the chordwise loading distribution was treated and stability achieved.[4]

The results of a number of theoretical calculations over a wide range of expanded area ratio have shown that the trends of the hydrodynamic forces and moments follow the experimental trends.[4] The magnitude of steady-state thrust and torque have been shown to agree within 5-8% and the magnitudes of unsteady thrust and torque within 5-15% with those of NSRDC experiments of a series of 3-blade propellers operating in an accurately measured screen-generated wake.

During the period of these investigations also, the computer program has been converted for the CDC 6600 high-speed digital computer so that the running time has been reduced considerably. Now information about steady-state and time-dependent propeller loading distributions and corresponding hydrodynamic forces and moments about blade bending moments and pressure signatures at various field points can be obtained in a comparatively short time.

Because of the availability of high speed digital computers the task previously considered formidable has been undertaken, viz., to improve the mathematical model by removing the so-called "staircase" approximation. A new kernel has been developed which takes into account the exact helicoidal wake and the exact blade geometry through the entire range of expanded area ratio. Thus an exact linearized version of the unsteady lifting surface theory as adapted to the propeller case is established.

A numerical procedure and corresponding computer program is developed here which will furnish the blade loading distribution and the resulting hydrodynamic forces and moments at any desired frequency. In addition, the program has the capability of evaluating blade bending moments about the pitch line at any radius and the pressure field around the operating propeller.

This study was sponsored by the Naval Ship Research and Development Center, Hydromechanics Research Program, Contract N00014-67-A-0202-0018.

LINEARIZED UNSTEADY LIFTING-SURFACE THEORY

The linearized unsteady lifting-surface theory for a marine propeller, with its blades lying on a helicoidal surface and operating in nonuniform flow of an incompressible, ideal fluid, was formulated by means of the acceleration-potential method in previous Davidson Laboratory papers. The development presented here is an adaptation of the previous developments, treating the helicoidal wake exactly as in Ref. 1, and incorporating all the improvements of the later papers, the exact blade geometry, a large number of chordwise modes, the "generalized lift-operator" technique.

It is known that evaluation of the blade loading distribution requires the solution of the following surface integral equation which relates the known velocity distribution to the unknown blade loading,

$$W(x,r,\varphi;t) = \iint_S L'(\xi,\rho,\theta;t)\, K(x,r,\varphi;\xi,\rho,\theta;t)\,dS \qquad \text{(i)}$$

where x, r, φ and ξ, ρ, θ: cylindrical coordinates of control and loading points, respectively

t: time, sec.

S: propeller surface, ft^2

W: known velocity distribution normal to propeller blades, ft/sec

L': unknown loading distribution, lb/ft^2

K: kernel function representing the self-induced velocity at a point on the blade due to unit amplitude load at each and every point on the blade, ft/lb-sec

The oscillatory loading and velocity distributions can be written as:

$$L'(\xi,\rho,\theta;t) = \sum_{\lambda=0}^{\infty} L'^{(\lambda)}(\xi,\rho,\theta)e^{i\lambda\Omega t} \tag{2}$$

$$W(x,r,\varphi;t) = \sum_{q=0}^{\infty} W^{(q)}(x,r,\varphi)e^{iq\Omega t} \tag{3}$$

where λ and q are positive integers and designate order of harmonic of the loading distribution and of the inflow field, respectively, the former to be determined by the analysis. The propeller rotates with angular velocity $-\Omega$.* The velocity W is caused by flow disturbances such as those due to hull wake, incidence angle or camber of the blades. In the linear theory their various effects are treated separately and simply added together.

The kernel function K has been developed in Ref. 6 without resorting to any geometric approximation. In that reference, which is concerned with two interacting propellers of counterrotating or tandem propulsive systems, a numerical procedure was suggested but not carried through to a computer program. Furthermore, treatment of numerical difficulties, such as the Cauchy-type singularity in the separable form of the kernel and a higher-order singularity with finite "Hadamard" contribution in the spanwise integration, was merely outlined or referenced. The present development follows that of Ref. 6 but with greater attention to detail.

DEVELOPMENT OF THE KERNEL FUNCTION

It is known that the pressure field generated by a lifting surface S is given by distributed doublets with axis parallel to the local normal, and with strength equal to the pressure jump across the surface S. Thus the pressure P at a point (x,r,φ) at time t will be given by

$$\Psi(x,r,\varphi;t) = \frac{1}{4\pi\rho_f} \iint_S \Delta P(\xi,\rho,\theta;t) \frac{\partial}{\partial n} \frac{1}{R'(x,r,\varphi;\ \xi,\rho,\theta)}\, dS \tag{4}$$

*minus sign for right-hand rotation (Ω has absolute value)

In Eq. (4), Ψ is the acceleration potential function defined as P/ρ_f

ρ_f fluid mass density

$\partial/\partial n$ normal derivative on the surface S at the loading point (ξ,ρ,θ)

$\vec{n}$ unit normal vector having positive axial component

$\Delta P(\xi,\rho,\theta;t)$ pressure jump across the lifting surface, i.e., $\Delta P = P_+ - P_-$, pressure difference between positive and negative oriented surfaces (with respect to x-axis)

$R'(x,r,\varphi;\xi,\rho,\theta)$ $[(x-\xi)^2 + r^2 + \rho^2 - 2r\rho\cos(\theta-\varphi)]^{\frac{1}{2}}$ = Descartes distance between the given control point and loading point

For doublets with pulsating strength $\Delta P(\xi,\rho,\theta)e^{i\omega t}$ at point (ξ,ρ,θ) which rotates with angular velocity $-\Omega$, Eq. (4) yields

$$\Psi(x,r,\varphi;t) = \frac{1}{4\pi\rho_f}\iint_S \Delta P(\xi,\rho,\theta)e^{i\omega t}\frac{\partial}{\partial n}\frac{1}{R'(x,r,\varphi;\xi,\rho,\theta_o-\Omega t)}dS \tag{5}$$

where ω = frequency, radians/sec

θ_o = angular position with respect to the blade midchord line

When the relation between velocity potential Φ and acceleration potential Ψ is utilized, viz.,

$$\Phi(x,r,\varphi;t) = -\frac{1}{U}\int_{-\infty}^{x}\Psi(\tau',r,\varphi;t-\frac{x-\tau'}{U})d\tau' \tag{6}$$

where U = forward velocity and the lifting surface is identified as the helicoidal surface of an N-bladed propeller, where both control and loading points rotate with angular velocity $-\Omega$, then the expression for the velocity potential is given by

$$\Phi(x,r,\varphi_o;t) = -\sum_{n=1}^{N}\sum_{\lambda=0}^{\infty}\frac{e^{i\lambda\Omega t}}{4\pi\rho_f U}$$

$$\cdot \iint_S \Delta P^{(\lambda)}(\xi,\rho,\theta_o)\int_{-\infty}^{x} e^{i\lambda[a(\tau'-x)-\bar{\theta}_n]}\frac{\partial}{\partial n}\left(\frac{1}{R}\right)d\tau' dS \qquad (7)$$

where $a = \Omega/U$

$\lambda = \omega/\Omega$, order of harmonic

$\bar{\theta}_n = 2\pi/N\,(n-1)$, $n = 1,2....N$

$R = \{(\tau'-\xi)^2 + r^2 + \rho^2 - 2r\rho\cos[\theta_o-\varphi_o+\bar{\theta}_n-a(\tau'-x)]\}^{\frac{1}{2}}$

φ_o = angular position of control point with respect to blade mid-chord line

The self-induced velocity at $(x,r,\varphi_o;t)$ on the helicoidal surface (i.e., R.H. side of Eq. (1)), will be given by

$$1. = \frac{\partial}{\partial n'}\Phi = -\sum_{n=1}^{N}\sum_{\lambda=0}^{\infty}\frac{e^{i\lambda\Omega t}}{4\pi\rho_f U}$$

$$\cdot \iint_S \Delta P^{(\lambda)}(\xi,\rho,\theta_o)\frac{\partial}{\partial n'}\int_{-\infty}^{x} e^{i\lambda[a(\tau'-x)-\bar{\theta}_n]}\frac{\partial}{\partial n}\left(\frac{1}{R}\right)d\tau' dS \qquad (8)$$

where $\frac{\partial}{\partial n'}$ is the normal derivative on the helicoidal surface at (x,r,φ), the control point.

The directional derivatives normal to the helicoidal surface, which is given by $x = \varphi_o/a$ or $\xi = \theta_o/a$, are:

$$\frac{\partial}{\partial n'} = \frac{r}{\sqrt{1+a^2r^2}}\left(a\frac{\partial}{\partial x} - \frac{1}{r^2}\frac{\partial}{\partial \varphi_o}\right) \qquad (9)$$

$$\frac{\partial}{\partial n} = \frac{\rho}{\sqrt{1+a^2\rho^2}} \left(a \frac{\partial}{\partial \xi} - \frac{1}{\rho^2} \frac{\partial}{\partial \theta_o}\right) \tag{10}$$

The L.H. of Eq. (1), viz.,

$$W(x,r,\varphi_o;t) = \sum_{q=0}^{\infty} W^{(q)}(x,r,\varphi_o)e^{iq\Omega t} = \sum_{q=0}^{\infty} V^{(q)}(r)e^{iq(\Omega t-\varphi_o)} \tag{11}$$

which is the known velocity distribution obtained from measurements, has time dependence of the form $e^{iq\Omega t}$, whereas the right-hand side, which is equivalent to Eq. (8), has time dependence of the form $e^{i\lambda\Omega t}$. This dictates that

$$\lambda = q$$

hence

$$1 = \iint_S L'^{(q)}(\rho,\theta_o)e^{iq\Omega t} K(r,\varphi_o;\rho,\theta_o;q)dS \tag{12}$$

where

$$L'^{(q)}(\rho,\theta_o) \equiv \Delta P^{(\lambda)}(\rho,\theta_o), \ \mathrm{lb/ft^2}$$

$$K = -\frac{1}{4\pi\rho_f U} \lim_{\delta\to 0} \sum_{n=1}^{N} e^{-iq\bar{\theta}_n} \frac{\partial}{\partial n'} \int_{-\infty}^{x} e^{iqa(\tau'-x)} \frac{\partial}{\partial n}\left(\frac{1}{R}\right)d\tau'$$

$$\delta = \frac{\varphi_o - \theta_o}{a} - (x - \xi) \tag{13}$$

and by $\delta \to 0$ is meant $x \to \varphi_o/a$ and $\xi \to \theta_o/a$. The limiting process is introduced to avoid the difficulty arising in the mathematical manipulation due to the high-order singularity.

The surface integral given by Eq. (12) is equivalent to

$$I = \int_{-\theta_b^\rho}^{\theta_b^\rho} \int_\rho \left\{L'^{(q)}(\rho, \theta_o) e^{iq\Omega t} K\right\} \frac{\sqrt{1+a^2\rho^2}}{a\rho} \rho d\rho d\theta_o \tag{14}$$

where θ_b^ρ is projected semichord length of the propeller blade at the loading point, in radians, and the factor $(\sqrt{1 + a^2\rho^2}/a\rho)$ is the result of changing the integration over the actual propeller blade to integration over its projection in the propeller plane. It should be noted that this does not correspond to placing the dipoles on the projection of the blade in the $x \equiv 0$ plane.

With the transformation

$$\theta_o = \sigma^\rho - \theta_b^\rho \cos\theta_\alpha \tag{15}$$

whwere θ_α is angular chordwise location of the loading point, and σ^ρ is angular position of the midchord line of the projected blade from the generator line through the hub (σ^ρ is a measure of skewness and is positive towards the trailing edge) and letting

$$L^{(q)}(\rho, \theta_o) \equiv L'^{(q)}(\rho, \theta_o)\, \rho\theta_b^\rho \quad (\text{lb/ft}) \tag{16}$$

the integral becomes

$$I = \int_0^\pi \int_\rho \left\{L^{(q)}(\rho, \theta_\alpha) e^{iq\Omega t} K\right\} \frac{\sqrt{1+a^2\rho^2}}{a\rho} \sin\theta_\alpha d\theta_\alpha\, d\rho \tag{17}$$

Use will be made of the following expansion scheme for the inverse Descartes distance

$$\frac{1}{R} = 1/\left\{(\tau'-\xi)^2 + r^2 + \rho^2 - 2r\rho\cos\beta\right\}^{\frac{1}{2}}$$

$$= \frac{1}{\pi} \sum_{m=-\infty}^{\infty} e^{im\beta} \int_{-\infty}^{\infty} I_m(|k|\rho)\, K_m(|k|r) e^{i(\tau'-\xi)k}\, dk \tag{18}$$

for $\rho < r$, where $I_m(\ )$ and $K_m(\ )$ are modified Bessel functions of the first and second kinds. For $\rho > r$, ρ and r are interchanged in the product of the modified Bessel functions. Here $\beta = \theta_o - \varphi_o + \bar{\theta}_n - a(\tau'-x)$.

After taking the derivatives as indicated in Eq. (13) and integrating over τ' (see Ref. 1), noting that

$$\sum_{n=1}^{N} e^{i(m-q)\bar{\theta}_n} = \begin{cases} N \text{ for } (m-q) = \ell N \quad \ell=0, \pm 1, \pm 2 \ldots \\ 0 \text{ for all other } m-q \end{cases}$$

the kernel function becomes for $\rho < r$

$$K(r,\varphi_o,\rho,\theta_o;q) = -\frac{N}{4\pi\rho_1 U}\frac{\rho r}{[(1+a^2\rho^2)(1+a^2r^2)]^{\frac{1}{2}}} \lim_{\delta\to 0} \sum_{\substack{m=-\infty \\ m=q+\ell N}}^{\infty} e^{im(\theta_o-\varphi_o)}$$

$$\cdot \Big\{ e^{ia(m-q)(x-\xi)}\left[a^2(m-q) + \frac{m}{r^2}\right]\left[a^2(m-q) + \frac{m}{\rho^2}\right] I_m(a|m-q|\rho)\, K_m(a|m-q|r)$$

$$- \frac{i}{\pi}\int_{-\infty}^{\infty}\left(ak + \frac{m}{r^2}\right)\left(ak + \frac{m}{\rho^2}\right)e^{ik(x-\xi)}\,\frac{I_m(|k|\rho)\,K_m(|k|r)}{k - a(m-q)}\,dk \Big\} \qquad (19)$$

It is obvious from Eq. (13) that in the limit as $\delta \to 0$, i.e., as $\varphi_o \to ax$ and $\theta_o \to a\xi$, R will go to zero when $\rho = r$, $\bar{\theta}_n = 0$ and $\tau' = 0$. Appendix A investigates this singular behavior of the kernel before and after the 1/R expansion of Eq. (18) and shows that the singularity is of high order with "Hadamard" finite contribution.

In addition, a Cauchy-type singularity is introduced in the k-integration of Eq. (19) through the series expansion of 1/R, which nevertheless is essential for the reduction of the surface integral equation (17) to a line integral equation. The kernel function is now in separable form which facilities the chordwise integration and permits use of the "generalized" lift operator technique for inverting the integral equation.

REDUCTION TO A ONE-DIMENSIONAL INTEGRAL EQUATION

The unknown loading $L^{(q)}(\rho,\theta_\alpha)$ of Eq. (17) will be approximated in the chordwise direction by the Birnbaum mode shapes

$$L^{(q)}(\rho,\theta_\alpha) = \frac{1}{\pi}\left\{L^{(q,1)}(\rho)\,\Theta(1) + \sum_{\bar{n}=2}^{\infty} L^{(q,\bar{n})}(\rho)\,\Theta(\bar{n})\right\} \tag{20}$$

where $L^{(q,\bar{n})}(\rho)$ are the spanwise loading components to be determined by the solution of the integral equation and

$$\Theta(1) = \cot\frac{\theta_\alpha}{2}$$

$$\Theta(\bar{n}) = \sin(\bar{n}-1)\theta_\alpha\,, \quad \bar{n} > 1 \tag{21}$$

Now after the limit is taken in Eq. (19) and with the trigonometric transformation of (15), the θ_α-integration can be performed analytically.

Both sides of the downwash integral equation are then operated on by the "generalized" lift operator, the structure of which is dictated by the separable form of the kernel (see Refs. 2 and 5). This method eliminates the φ_o-dependence of the integral equation. Thus a set of line integral equations is obtained with maximum order of lift operator $\bar{m}$ equal to maximum number of unknown chordwise modes $\bar{n}$. The solution of the $\bar{m} = \bar{n}$ integral equations is obtained by the collocation method.

With the transformation

$$\varphi_o = \sigma^r - \theta_b^r \cos\varphi_\alpha$$

where φ_α is angular chordwise location of the control point and the superscript r refers to values at the radial location of the control point, the non-dimensionalized downwash integral equation is reduced to the following form for each $q \geq 0$ and each $\bar{m} = 1, \ldots \bar{n}_{max}$:

$$\frac{\bar{W}^{(q,\bar{m})}(r)}{U} = \sum_{\bar{n}=1}^{\bar{n}max} \int_{\rho} L^{(q,\bar{n})}(\rho)\ \bar{K}^{(\bar{m},\bar{n})}\ (r,\rho;q)d\rho \tag{22}$$

where from Eq. (11)

$$\bar{W}^{(q,\bar{m})}(r) = \frac{1}{\pi}\int_{o}^{\pi} \Phi(\bar{m})\ W^{(q)}(r,\varphi_o)d\varphi_\alpha \tag{23}$$

$$\bar{K}^{(\bar{m},\bar{n})}(r,\rho;q) = \frac{1}{\pi^2}\int_{o}^{\pi}\int_{o}^{\pi} \Phi(\bar{m})\ \Theta(\bar{n})\ \frac{K(r,\varphi_o;\rho,\theta_o q)}{U}\ \frac{\sqrt{1+a^2\rho^2}}{a\rho}\ \sin\theta_\alpha d\theta_\alpha d\varphi_\alpha \tag{24}$$

and the lift operator function $\Phi(\bar{m})$ is

$$\Phi(1) = 1 - \cos\varphi_\alpha \quad \text{(the Glauert lift operator)}$$

$$\Phi(2) = 1 + 2\cos\varphi_\alpha$$

$$\Phi(\bar{m}) = \cos(\bar{m}-1)\varphi_\alpha \quad \text{for } \bar{m} > 2 \tag{25}$$

In explicit form, Eq. (23) becomes:

$$\frac{\bar{W}^{(q,\bar{m})}(r)}{U} = \frac{V^{(q)}(r)}{U}\ e^{-iq\sigma^r}\ I^{(\bar{m})}(q\theta_b^r) \tag{26}$$

where $I^{(\bar{m})}(q\theta_b^r) = \frac{1}{\pi}\int_{o}^{\pi} \Phi(\bar{m})e^{iq\theta_b^r\cos\varphi_\alpha}d\varphi_\alpha$

The latter is evaluated in Appendix B.

The modified kernel function, after the chordwise integrations, is for $\rho < r$

$$\bar{K}^{(\bar{m},\bar{n})} = \left\{ \frac{-N}{4\pi\rho_f U^2 r_o} \right\} \frac{r}{a\sqrt{1+a^2 r^2}} \sum_{\substack{m=-\infty \\ m=q+\ell N}}^{\infty} e^{-im\Delta\sigma}$$

$$\cdot \left\{ e^{i(m-q)\Delta\sigma} \left[a^2(m-q) + \frac{m}{r^2}\right] \left[a^2(m-q) + \frac{m}{\rho^2}\right] I^{(\bar{m})}(q\theta_b^r)\Lambda^{(\bar{n})}(q\theta_b^\rho) \right.$$

$$\cdot\ I_m(|m-q|\rho)\ K_m(|m-q|r)$$

$$\left. - \frac{1}{\pi}\int_{-\infty}^{\infty} \left(ak+\frac{m}{r^2}\right)\left(ak+\frac{m}{\rho^2}\right) e^{i\frac{k}{a}\Delta\sigma} \frac{I^{(\bar{m})}\left(\left(m-\frac{k}{a}\right)\theta_b^r\right)\Lambda^{(\bar{n})}\left(\left(m-\frac{k}{a}\right)\theta_b^\rho\right)}{k-a(m-q)} I_m(|k|\rho)K_m(|k|r)dk \right\} \tag{27}$$

where $\Lambda^{(\bar{n})}(x) = \frac{1}{\pi}\int_0^{\pi} \Theta(\bar{n}) e^{-ix\cos\theta_\alpha} \sin\theta_\alpha d\theta_\alpha$ which is also evaluated in Appendix B. In Eq. (27) all terms outside the first braces are non-dimensionalized with respect to r_o, as is also ρ in Eq. (22), and $\Delta\sigma = \sigma^r - \sigma^\rho$.

Let $\lambda = k - a\ell N$, then the k-integral of Eq. (27) is

$$I_k = e^{i\ell N\Delta\sigma} \int_{-\infty}^{\infty} \frac{g(\lambda)d\lambda}{\lambda} = e^{i\ell N\Delta\sigma} \int_0^{\infty} \frac{g(\lambda)-g(-\lambda)}{\lambda} d\lambda \tag{28}$$

where

$$g(\lambda) = (IK)_m\ B_{\bar{m},\bar{n}}(\lambda) e^{i\frac{\lambda}{a}\Delta\sigma}$$

$$(IK)_m = \begin{cases} I_m(|\lambda+a\ell N|\rho)\ K_m(|\lambda+a\ell N|r) & \text{for } \rho < r \\ I_m(|\lambda+a\ell N|r)\ K_m(|\lambda+a\ell N|\rho) & \text{for } \rho > r \end{cases}$$

$$B_{\bar{m},\bar{n}}(\lambda) = \left(a\lambda+a^2\ell N+\frac{m}{r^2}\right)\left(a\lambda+a^2\ell N+\frac{m}{\rho^2}\right) I^{(\bar{m})}\left(\left(q-\frac{\lambda}{a}\right)\theta_b^r\right)\Lambda^{(\bar{n})}\left(\left(q-\frac{\lambda}{a}\right)\theta_b^\rho\right)$$

Equation (28) has an integrable singularity at $\lambda = 0$. The value of the integrand at this singularity is obtained by L'Hospital's rule, as shown in Appendix C:

a) when $\lambda = 0$ and $\ell \neq 0$

$$\lim_{\lambda\to 0}\left[\frac{g(\lambda)-g(-\lambda)}{\lambda}\right. = 2\left\{(IK)_m\Big|_{\lambda=0}\left(\frac{i\Delta\sigma}{a}B_{\bar{m},\bar{n}}(0) + \frac{\partial B_{\bar{m},\bar{n}}(\lambda)}{\partial\lambda}\Big|_{\lambda=0}\right)\right.$$

$$\left. \pm B_{\bar{m},\bar{n}}(0)\,\frac{\partial(IK)_m}{\partial\lambda}\Big|_{\lambda=0}\right\} \tag{29a}$$

where the upper sign is taken when $\ell > 0$ and the lower when $\ell < 0$, and the derivatives are given in Appendix C.

b) when $\lambda = 0$, $\ell = 0$ and $m = q = 0$

$$\lim_{\lambda\to 0}\left[\frac{g(\lambda) - g(-\lambda)}{\lambda}\right] = 0 \tag{29b}$$

c) when $\lambda = 0$, $\ell = 0$ and $m = q \neq 0$

$$\lim_{\lambda\to 0}\left[\frac{g(\lambda) - g(-\lambda)}{\lambda}\right] = 2\left\{\lim_{\ell\to 0}(IK)_m\Big|_{\lambda=0}\right\}$$

$$\cdot\left\{\left[\frac{i\Delta\sigma}{a}\frac{m^2}{r^2\rho^2} + am\left(\frac{1}{r^2}+\frac{1}{\rho^2}\right)\right] I^{(\bar{m})}(q\theta_b^r)\Lambda^{(\bar{n})}(q\theta_b^\rho)\right.$$

$$\left. - \frac{im^2}{ar^2\rho^2}\left[\theta_b^r I_1^{(\bar{m})}(q\theta_b^r)\Lambda^{(\bar{n})}(q\theta_b^\rho) - \theta_b^\rho I^{(\bar{m})}(q\theta_b^r)\Lambda_1^{(\bar{n})}(q\theta_b^\rho)\right]\right\} \tag{29c}$$

where

$$\lim_{\ell\to 0}(IK)_m\Big|_{\lambda=0} = \begin{cases} \dfrac{1}{2|m|}\left(\dfrac{\rho}{r}\right)^{|m|} & \text{for } \rho < r \\[2ex] \dfrac{1}{2|m|}\left(\dfrac{r}{\rho}\right)^{|m|} & \text{for } \rho > r \end{cases}$$

and $I_1^{(\bar{m})}(x)$ and $\Lambda_1^{(\bar{n})}(x)$ are defined in Appendix B.

Equation (27) can now be written as

$$K^{(\bar{m},\bar{n})} = \left\{\frac{-N}{4\pi\rho_f U^2 r_o}\right\} \frac{r\, e^{-iq\Delta\sigma}}{a\sqrt{1+a^2r^2}} \sum_{\substack{m=-\infty \\ m=q+\ell N}}^{\infty} \left\{g(0) - \frac{1}{\pi}\int_0^{\infty} \frac{g(\lambda)-g(-\lambda)}{\lambda}\, d\lambda\right\} \quad (30)$$

where

$$g(0) = (IK)_m\Big|_{\lambda=0} \left\{\left(a^2\ell N + \frac{m}{r^2}\right)\left(a^2\ell N + \frac{m}{\rho^2}\right) I^{(\bar{m})}(q\theta_b^r)\Lambda^{(\bar{n})}(q\theta_b^\rho)\right\}$$

For large $|\lambda| \geq U_F$, the integrand of Eq. (30) tends to zero. For large argument $|\pm\lambda + a\ell N|$ (ρ or r) of the modified Bessel functions,

$$(IK)_m \text{ of (28)} \approx \frac{e^{-|\pm\lambda+a\ell N|\,|r-\rho|}}{2\sqrt{r\rho}\,|\pm\lambda+a\ell N|}$$

so that

$$\frac{g(\pm\lambda)}{\lambda} \approx \frac{e^{-|\pm\lambda+a\ell N|\,|r-\rho|}}{2\sqrt{r\rho}\,\lambda|\pm\lambda+a\ell N|}\; a^2\left(\pm\lambda+a\ell N + \frac{m}{ar^2}\right)\left(\pm\lambda+a\ell N+\frac{m}{a\rho^2}\right)e^{\pm i\frac{\lambda}{a}\Delta\sigma}$$

$$\cdot\, I^{(\bar{m})}\left(\left(q\mp\frac{\lambda}{a}\right)\theta_b^r\right)\Lambda^{(\bar{n})}\left(\left(q\mp\frac{\lambda}{a}\right)\theta_b^\rho\right) \quad (31)$$

If λ and $a\ell N$ are opposite in sign and $|\lambda| \to |a\ell N|$, i.e., the arguments are small, then

$$(IK)_m \approx \frac{1}{2|m|} z^{|m|}$$

where $z = \rho/r$ for $\rho < r$ and $z = r/\rho$ for $\rho > r$. In this case

$$\frac{g(\pm\lambda)}{\lambda} \approx \frac{1}{2|m|} z^{|m|} \frac{m^2}{\lambda r^2 \rho^2} e^{\pm i\frac{\lambda}{a}\Delta\sigma}\, I^{(\bar{m})}\left(\left(q\mp\frac{\lambda}{a}\right)\theta_b^r\right)\Lambda^{(\bar{n})}\left(\left(q\mp\frac{\lambda}{a}\right)\theta_b^\rho\right) \quad (32)$$

When λ is large, the product of the $I^{(\bar{m})}$ and $\Lambda^{(\bar{n})}$ functions varies as $1/\lambda$. Equation (31) is seen to be negligibly small for large λ provided that $|m| = |q+\ell N|$ is not too much larger than λ, for example if $a\ell N$ is smaller

than λ^2. Equation (32) tends to zero for both large λ and large $|m| \geq M_F$ since $|\lambda| \rightarrow |a\ell N|$.

The integral equation given by Eq. (22) with the kernel given by Eq. (32) can be solved numerically by the usual collocation method. In this method the loading $L^{(q,\bar{n})}(\rho)$ is assumed to be constant over each small radial strip, 2β in length. Then only the kernel needs to be integrated over the radial strip. When $\rho \neq r$ the integration of the kernel in the range $\rho_i - \beta < \rho < \rho_i + \beta$ is performed by the tangential method.

In the radial strip $r - \beta < \rho < r + \beta$ which includes $\rho = r$, a high-order singularity occurs, as noted in Appendix A. Its "Hadamard" finite contribution is evaluated by the Lagrange interpolation method described in Appendix D, as suggested by Mangler.[9]

PROPELLER LOADING AND RESULTING FORCES AND MOMENTS

Loading

The downwash integral equation (22) is solved for propeller loadings $L^{(q,\bar{n})}(\rho)$ due to the known velocity distribution $\bar{W}^{(q,\bar{m})}(r)$ normal to the blades. The velocity distribution of Eq. (26) is the hull-induced distribution at shaft frequencies q obtained from wake surveys in the propeller plane. To the loadings due to these wake velocities are added loadings arising from various disturbances imposed on this flow.

The propeller blades do not coincide with the assumed helicoidal surface of pitch 1/a but are located on a nearby surface of pitch P(r) and furthermore they are cambered. (As in previous Davidson Laboratory papers, thickness is neglected.) The velocities induced by the flow-incidence angle and camber effects are independent of time because the blades are considered rigid, so that only the steady-state loading (q = 0) will be affected. For the flow angle effect the left-hand side of the integral equation is replaced by

$$\frac{\bar{V}_f^{(o,\bar{m})}(r)}{U} = -\sqrt{1 + a^2 r^2}\left(\tan^{-1}\frac{P(r)}{2\pi r} - \tan^{-1}\frac{1}{ar}\right) \text{ for } \bar{m} = 1,2$$

$$= 0 \text{ for } \bar{m} > 2 \qquad (33)$$

(since this effect depends only on radial position and not on φ_α) where the incident flow angle is defined by the difference between the actual geometric pitch angle $\theta_p(r) = \tan^{-1}(P/2\pi r)$ and the hydrodynamic pitch angle $\tan^{-1}(1/ar)$ of the assumed surface.

For the camber effect the left-hand side of the integral equation is

$$\frac{\bar{v}_c^{(o,\bar{m})}(r)}{U} = \frac{\sqrt{1+a^2r^2}}{2\pi b(r)} \int_o^\pi \Phi(\bar{m}) \frac{\partial f(r,s)}{\partial s} d\varphi_\alpha$$

$$= \frac{\sqrt{1+a^2r^2}}{\pi b(r)} \int_o^\pi \Phi(\bar{m}) \frac{\partial f}{\partial \varphi_\alpha} \frac{d\varphi_\alpha}{\sin\varphi_\alpha} \tag{34}$$

where $b(r)$ = semichord, ft.

$\frac{\partial f(r,s)}{\partial s}$ = slope of camberline $f(r,s)$ given at discrete points measured from face pitch line

s = $(1-\cos\varphi_\alpha)/2$, chordwise location nondimensionalized on basis of $2b(r)$

The evaluation of integral (34) is given in Reference 4 for arbitrary blade camber shape.

Once the values of $L^{(q,\bar{n})}$ due to the various disturbances are determined the spanwise loading distribution follows from Eq. (20):

$$L^{(q)}(r) = \int_o^\pi L^{(q)}(r,\theta_\alpha)\sin\theta_\alpha d\theta_\alpha$$

$$= \frac{1}{\pi}\int_o^\pi \left\{L^{(q,1)}(r)(1+\cos\theta_\alpha) + \sum_{\bar{n}=2}^{\infty} L^{(q,\bar{n})}(r)\sin(\bar{n}-1)\theta_\alpha \sin\theta_\alpha\right\} d\theta_\alpha$$

$$= L^{(q,1)}(r) + \frac{1}{2}L^{(q,2)}(r) \tag{35}$$

Propeller-Generated Forces and Moments

With the principal components of the propeller-induced forces and moments defined as follows

Forces: F_x = thrust (x-direction)

F_y and F_z = horizontal and vertical components, respectively, of the bearing forces

Moments: Q_x = torque about the x-axis

Q_y and Q_z = bending moments about the y- and z-axis, respectively

the total forces at frequency $\ell N(\ell=0,1,2,\ldots)$ acting on an N-bladed propeller will be given by (cf. Ref. 3)

$$F_x = \mathrm{Re}\left\{Nr_o\, e^{i\ell N\Omega t} \int_0^1 L^{(\ell N)}(r)\cos\theta_p(r)\,dr\right\}$$

$$F_y = \mathrm{Re}\left\{\frac{Nr_o}{2}\, e^{i\ell N\Omega t} \int_0^1 \left[L^{(\ell N-1)}(r)+L^{(\ell N+1)}(r)\right]\sin\theta_p(r)\,dr\right\} \tag{36}$$

$$F_z = \mathrm{Re}\left\{\frac{Nr_o}{2i}\, e^{i\ell N\Omega t} \int_0^1 \left[L^{(\ell N-1)}(r)-L^{(\ell N+1)}(r)\right]\sin\theta_p(r)\,dr\right\}$$

(with the sign convention adopted in the present investigation).

The moments are determined by

$$Q_x = -\,\mathrm{Re}\left\{Nr_o^2\, e^{i\ell N\Omega t} \int_0^1 L^{(\ell N)}(r)\sin\theta_p(r)\,r\,dr\right\}$$

$$Q_y = \mathrm{Re}\left\{\frac{Nr_o^2}{2}\, e^{i\ell N\Omega t} \int_0^1 \left[L^{(\ell N-1)}(r)+L^{(\ell N+1)}(r)\right]\cos\theta_p(r)\,r\,dr\right\} \tag{37}$$

$$Q_z = \mathrm{Re}\left\{\frac{Nr_o^2}{2i}\, e^{i\ell N\Omega t} \int_0^1 \left[L^{(\ell N-1)}(r)-L^{(\ell N+1)}(r)\right]\cos\theta_p(r)\,r\,dr\right\}$$

It may be observed from the foregoing that the propeller-generated transverse forces and bending moments are evaluated from propeller loadings associated with wake harmonics at frequencies adjacent to blade frequency, i.e., at $q = \ell N \pm 1$, whereas the thrust and torque are determined by the loading at blade frequency. The steady-state thrust and torque are determined at zero frequency; the corresponding mean transverse forces and bending moments are determined at shaft frequency.

Blade Bending Moments

The blade bending moment about the face pitch line at any radius r_j of a blade is calculated from $L^{(q)}(r)$ at any shaft frequency q as

$$M_b^{(q)} = r_o^2\, e^{iq\Omega t} \int_{r_j}^1 L^{(q)}(r)\cos[\theta_p(r)-\theta_p(r_j)]\,(r-r_j)\,dr \tag{38}$$

The total vibratory blade bending moment distribution is then obtained from

$$M_b = \mathrm{Re} \sum_q M_b^{(q)} \, e^{iq\Omega t} \tag{39}$$

The computer program, which implements the numerical procedure developed here, furnishes the blade loading distributions (Eq. 35), the hydrodynamic forces and moments (Eqs. 36-37), and the blade bending moment distribution (Eqs. 38 and 39).

The program also implements the procedure developed in Ref. 10 for the evaluation of the propeller-induced vibratory pressure field from the blade loadings $L^{(q,\bar{n})}(\rho)$. The blade-frequency pressures due to loading, are shown to be of the form

$$p^{(\ell N)} = \sum_{\bar{n}=1}^{\infty} \sum_{\mu=0}^{\infty} \sum_{\rho} \left\{ L^{(\mu,\bar{n})}(\rho) k^{(\mu-\ell N,\bar{n})} + \text{conj.} \left[L^{(\mu,\bar{n})}(\rho) k^{(\mu+\ell N,\bar{n})} \right] \right\} \tag{40}$$

where the k functions are the so-called influence functions connecting the loading points on the blade with the space points.

Also available from Ref. 10 is a computational procedure to determine the blade thickness effects on the pressure field. Although these effects are negligibly small in the case of bearing forces, they are demonstrably large in the pressure field in the neighborhood of the operating propeller.

NUMERICAL RESULTS

Using the present development with exact treatment of the helicoidal wake from the blades, systematic calculations of steady and unsteady blade loading and hydrodynamic forces and moments were made for a series of 3-bladed propellers of expanded area ratio EAR between 0.3 and 1.2. These propellers were chosen because they were subjects of earlier papers[3,4] which had used the "staircase" approximation of the wake, and because experimental data for the three propellers of EAR, 0.3, 0.6 and 1.2, were available from controlled NSRDC tests in nonuniform flow with wake structure rigidly specified and vibratory forces made large to minimize experimental error.

The tests had been conducted in the NSRDC 24-inch water tunnel using the closed-jet test section with a screen to produce the wake, a 3-cycle screen for the force along and moment about the longitudinal axis and a 4-cycle screen for the forces along and moments about the transverse and vertical axes. The tests were run at a constant speed of 15 rps with free stream velocity close to 12.5 ft/sec. The design mean thrust coefficient $\bar{K}_T$ was 0.150 (practically open-water value in the 3-cycle screen wake).

The propellers, with destroyer-type blade outlines and modified NACA-66 section with a = 0.8 mean line, were one foot in diameter with hub diameter 0.2 ft and pitch ratio 1.08 at .7 radius. For the propellers at other expanded area ratios the pitch variation along the span, RPM and flow velocity normal to the blade were considered to be the same and equal to the corresponding values for the propeller of EAR = 0.6 (taken as the norm). The camberline variations were determined by linear interpolation of the known ratios of maximum camber to chord m_x/c shown in the table below for the propellers with EAR = 0.3, 0.6 and 1.2.

TABLE 1

Ratio of Maximum Camber to Chord, m_x/c

Radius	EAR = 0.3	EAR = 0.6	EAR = 1.2
.25	.0370	.0228	.0196
.35	.0388	.0231	.0202
.45	.0372	.0224	.0196
.55	.0340	.0212	.0185
.65	.0312	.0203	.0177
.75	.0290	.0198	.0170
.85	.0270	.0189	.0160
.95	.0247	.0174	.0147

The results of the calculations are shown in Figures 1-4 and Tables 2 and 3. Figure 1 compares the mean thrust coefficients evaluated by the present method with the earlier computations using the "staircase" approximation of the blade wake, and with the experimental value of 0.15. As can be seen, with the exception of the propeller of 0.3 EAR, the present

calculations are closer to the measurements. Repeating the calculations with finer mesh and higher limits for the integration has not changed the result. The approximately 13% increase in mean thrust at EAR = 0.3 reflects the disproportionately large camber employed with the small blade area ratio (see Table 1).

It is to be remembered that the blade thickness effect on the loading has been neglected here as in the previous studies. This effect, which is expected to decrease the calculated mean thrust, is probably insignificant in most cases, but may be large enough in the case of the unusually thick propeller of 0.3 EAR to bring the value closer to experiment. This is the subject of a current investigation at the Davidson Laboratory.

The steady-state spanwise loading distributions are presented in Figure 2 in terms of EAR. At all EAR the loading is shown to increase with radius from 0.25 to 0.85 and then decrease at 0.95. The trends versus EAR at every radius with the exception of 0.95 are consistent. The rise in all curves at EAR = 0.3 is reflected in the higher mean thrust coefficient for that propeller.

Figure 3 compares the blade-frequency vibratory thrust and torque amplitudes computed by the present method with the earlier calculations reported in Reference 4 which used the "staircase" approximation of the blade wake, and with the experimental values. The present theoretical results are quite close to the test data. The proportionately greater improvement in the torque amplitudes over the earlier calculations is especially gratifying since it indicates that the radial load distributions are more accurately determined.

Figure 4 presents the real and imaginary parts of these radial loading distributions versus EAR at first blade frequency q = N = 3. The distributions show smooth trends with EAR, and a definite pattern with increasing radius from 0.25 to 0.85. At 0.95 radius the trend is completely different. The curves of loading as a function of EAR are similar to those shown in Ref. 4, Figure 10, but are lower in magnitude and without the inflections at high EAR of the earlier calculations.

A comparison of the blade-frequency amplitudes of nondimensional transverse and vertical force coefficients and coefficients of moments about the transverse and vertical axes from NSRDC measurements and the theory is given in Table 2. The coefficients are for the 3-bladed propellers tested in a 4-cycle screen-generated wake at the design advance ratio J. (The resolution of forces and moments is shown in Fig. 5.)

TABLE 2

Experimental and Theoretical Transverse and Vertical Force and Moment Coefficients for a Set of 3-Bladed Propellers

	EAR = 0.3		EAR = 0.6		EAR = 1.2	
Amp. x 10^2	Exp.	Theory	Exp.	Theory	Exp.	Theory
$\tilde{K}_{F_y}$	1.08	0.96	1.34	0.98	0.77	0.40
$\tilde{K}_{F_z}$	1.04	0.95	1.25	1.06	0.57	0.69
$\tilde{K}_{Q_y}$	0.92	0.87	1.10	0.93	0.77	0.40
$\tilde{K}_{Q_z}$	0.89	0.83	1.06	0.93	0.70	0.53

A comparison of the corresponding phase angles is given in Table 3 which also presents the phase angles for blade-frequency thrust and torque.

TABLE 3

φ, Phase Angle in Degrees

	EAR = 0.3		EAR = 0.6		EAR = 1.2	
Vibratory Forces	Exp.	Theory	Exp.	Theory	Exp.	Theory
$\tilde{F}_x$	207	222	238	257	323	331
$\tilde{Q}_x$	205	42*	234	77*	310	151*
$\tilde{F}_y$	351	153*	32	204*	164	332*
$\tilde{Q}_y$	356	148*	31	191*	100	288*
$\tilde{F}_z$	255	255	293	308	77	67
$\tilde{Q}_z$	262	247	294	292	2	34

*Approximately 180 deg. out-of-phase with experiment.

Knowing the magnitude M and phase angle φ of a particular force or moment its cosine and sine components can be determined by means of the expression

$$M \cos(q\Omega t - \varphi)$$

This form is also useful in establishing the lead or lag of the quantity with respect to the sinusoidal input wake at a specified radial position or the location of a maximum relative to the rotating blade.

For all the transverse and vertical force and moment coefficients the trends with EAR of measured and theoretical values are similar. However, the correlation between experimentally and theoretically derived coefficients is not as good as that for the vibratory thrust and torque.

Examples of propeller blade chordwise loading distributions are shown in Figures 6 and 7 for the two extremes of expanded area ratio, 0.3 and 1.2. These figures compare the distributions obtained by the normal sum of the Birnbaum chordwise modes (up to finite $\bar{n} = M$) viz.

$$S_{\bar{n}} = L^{(1)}(r) \cot \frac{\theta_\alpha}{2} + \sum_{n=2}^{M} L^{(\bar{n})}(r) \sin(\bar{n}-1)\theta_\alpha \tag{41}$$

with the Cesaro sum

$$\sigma_{\bar{n}} = L^{(1)}(r) \cot \frac{\theta_\alpha}{2} + \sum_{\bar{n}=2}^{M} \left(\frac{M-\bar{n}+2}{M}\right) L^{(\bar{n})}(r) \sin(\bar{n}-1)\theta_\alpha \tag{42}$$

The Cesaro summability is a proper procedure for obtaining the limit of slowly convergent or even divergent series. Use of this method in Ref. 4, where calculations of loading were based on the "staircase" approximation of the blade wake, served to stabilize the chordwise distribution which was particularly erratic in the neighborhood of the leading edge for large EAR (>1).

The Cesaro and normal sums in Figs. 6 and 7 are both smooth and close in value. This is an indication that removal of the "staircase" approximation with the present exact treatment of the blade wake results in a more rapidly converging series, and consequently in a smoother chordwise distribution.

CONCLUSION

The theory which was developed in Ref. 2 in adapting the unsteady lifting surface theory to the marine propeller case has been revised by removing the so-called "staircase" approximation describing the blade wake. The present "exact" mathematical model takes cognizance of the exact helicoidal geometry of the propeller blade and its wake, as well as the presence of interacting blades and the fact that the propeller operates in nonuniform flow (hull wake). A new numerical procedure has been devised and programmed for the CDC 6600 high-speed digital computer primarily for the calculation of the blade loading distributions at various shaft frequencies. The resulting hydrodynamic forces and moments are evaluated from the loading distributions: thrust and torque, steady and time-dependent, from the loading at zero frequency and multiples of blade frequency, the other bearing forces and moments, transverse and vertical, from the loading at first shaft frequency for the steady-state case and from the loadings at one above and one below blade frequencies for the time-dependent cases. In addition, the program has the capability of calculating the vibratory blade bending moment about the face pitch line at any radius and the pressure field due to the loading of the propeller when it operates in uniform or nonuniform inflow fields.

The results of this new approach with the exact helicoidal blade wake have not shown any dramatic changes from the results of previous calculations. However, it can be stated that an overall improvement has been witnessed in the correlation of forces and moments with experimental measurements, which indicates that the radial loading distributions are more accurately determined. The detailed loading distributions, both radial and chordwise, are much smoother than obtained in the previous calculations by means of the "staircase" model.

Other unreported calculations for propellers in the wake of a ship, rather than in the strong blade-frequency wake generated by a screen, have shown little difference in the results by both methods except in

the steady-state case where the new method yields results closer to the experimental values.

Unfortunately the machine running time has increased considerably, calculations taking about 4 to 5 times longer. It is felt, at this stage, that numerical simplifications and other approximations should not be attempted before extensive use of this program can be made for a better understanding of the importance of the various contributions to the solution.

It is suggested for the present that if detailed and accurate information is required, the program of the "exact" mathematical model should be utilized, whereas when integrated effects like forces and moments are desired the "staircase" model is adequate. This statement applies especially when the relative merits and disadvantages of propeller settings are under consideration.

REFERENCES

1. Tsakonas, S., Chen, C.Y. and Jacobs, W.R., "Exact Treatment of the Helicoidal Wake in the Propeller Lifting-Surface Theory," DL Report 1117, Stevens Institute of Technology, August 1966; J. Ship Research Vol. 11, No. 3, September 1967, pp. 154-170.

2. Tsakonas, S., Jacobs, W.R., and Rank, P., "Unsteady Propeller Lifting Surface Theory with Finite Number of Chordwise Modes," DL Report 1133, Stevens Institute of Technology, December 1966; J. Ship Research Vol. 12, No. 1, March 1968, pp. 14-46.

3. Tsakonas, S., Breslin, J.P. and Miller, M., "Correlation and Application of an Unsteady Flow Theory for Propeller Forces," Transactions of SNAME Vol. 75, 1967.

4. Tsakonas, S. and Jacobs, W.R , "Propeller Loading Distributions," DL Report 1319, Stevens Institute of Technology, August 1968; J. Ship Research Vol. 13, No. 4, December 1969, pp. 237-258.

5. Jacobs, W R. and Tsakonas, S., "Generalized Lift Operator Technique for the Solution of the Downwash Integral Equation," DL Report 1308, Stevens Institute of Technology, August 1968. Published as "A New Procedure for the Solution of Lifting Surface Problems," J. Hydronautics Vol. 3, No. 1, January 1969, pp. 20-28.

6. Tsakonas, S. and Jacobs, W.R., "Counterrotating and Tandem Propellers Operating in Spatially Varying, Three-Dimensional Flow Fields, Part I - Analysis," DL Report 1335, Stevens Institute of Technology, September 1968.

7. Nicholson, J.W., "The Approximate Calculations of Bessel Functions of Imaginary Argument," Phil. Mag., Series 6, Vol. 20, December 1910, pp. 938-943.

8. Jolley, L.B.W., ed., Summation of Series, Dover Publications, Inc., New York, 1961.

9. Mangler, K.W., "Improper Integrals in Theoretical Aerodynamics," British Royal Aircraft Establishment, Aero 2424, ARC 14, 394, 1959.

10. Jacobs, W.R., Mercier, J. and Tsakonas, S., "Theory and Measurements of the Propeller-Induced Vibratory Pressure Field," Report SIT-DL-70-1485, Stevens Institute of Technology, November 1970. To be published in J. of Ship Research.

11. Scarborough, J.B., Numerical Mathematical Analysis, The Johns Hopkins Press, Baltimore, Md., 1958.

12. Watkins, C.E., Woolston, D.S. and Cunningham, H.J., "A Systematic Kernel Function Procedure for Determining Aerodynamic Forces on Oscillating or Steady Finite Wings at Subsonic Speeds," NASA Technical Report R-48, 1959.

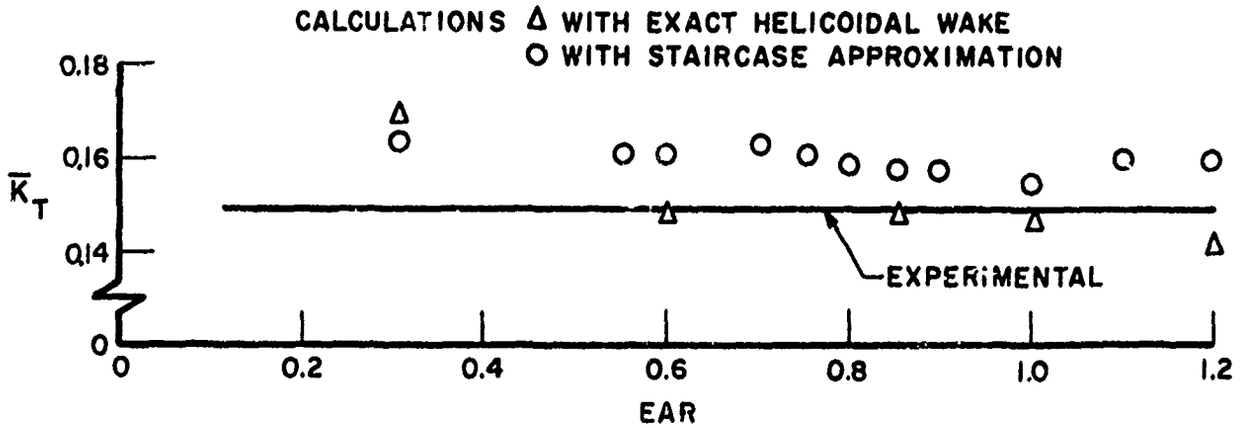

FIG. 1. MEAN THRUST COEFFICIENTS FOR 3-BLADED PROPELLERS

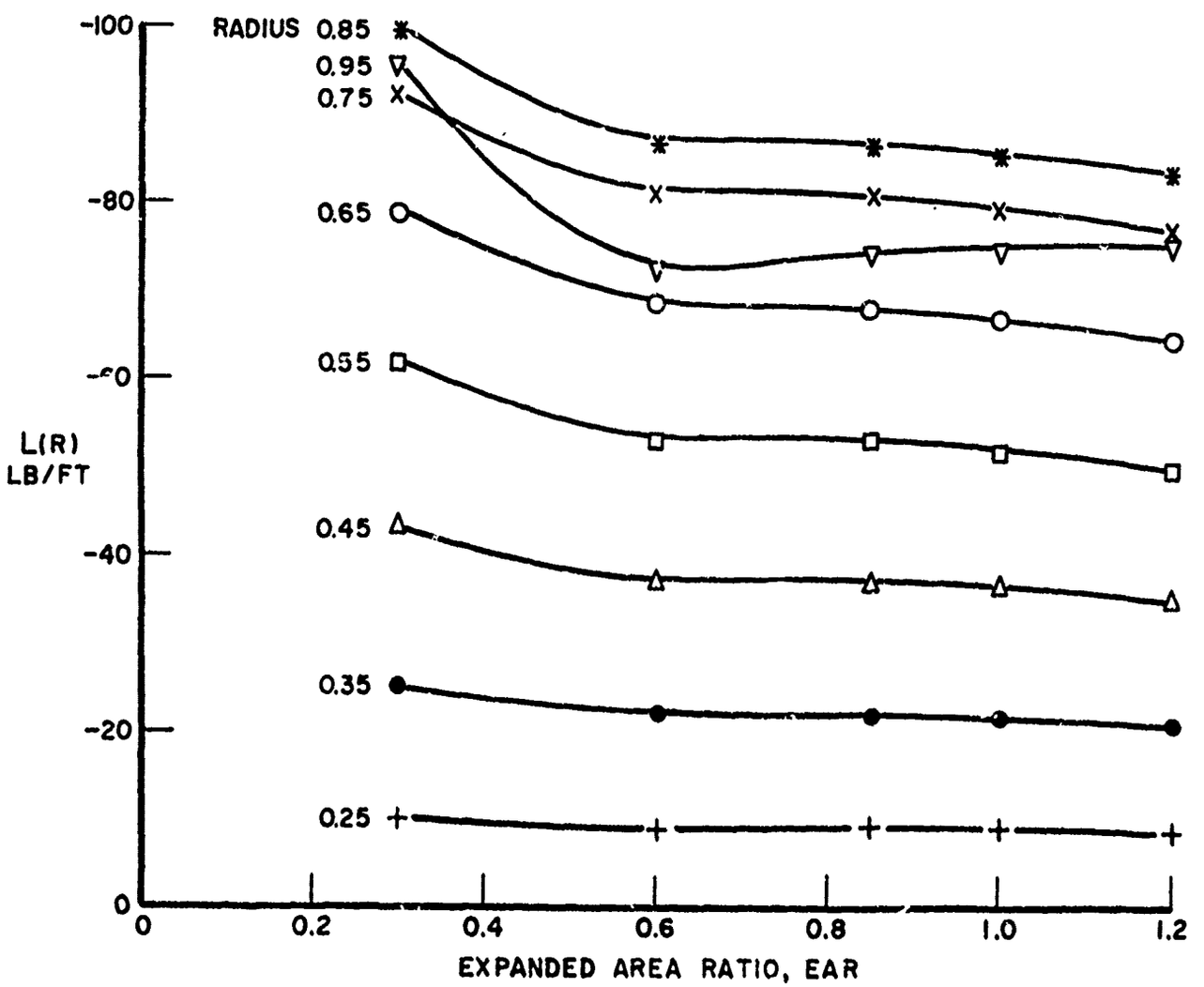

FIG. 2 STEADY-STATE SPANWISE LOADINGS FOR 3-BLADED PROPELLERS

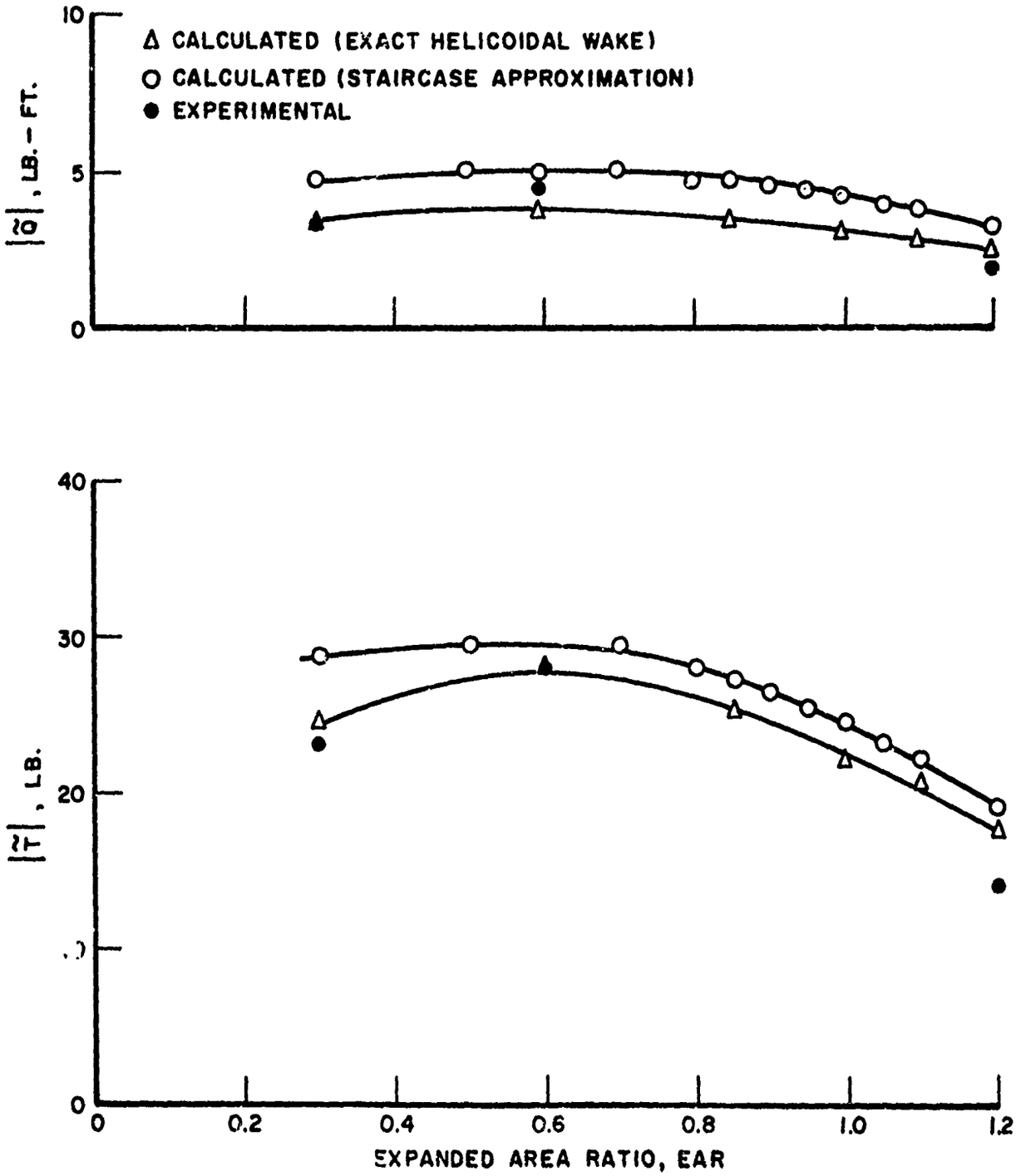

FIG. 3. AMPLITUDES OF VIBRATORY THRUST AND TORQUE FOR 3-BLADED PROPELLERS

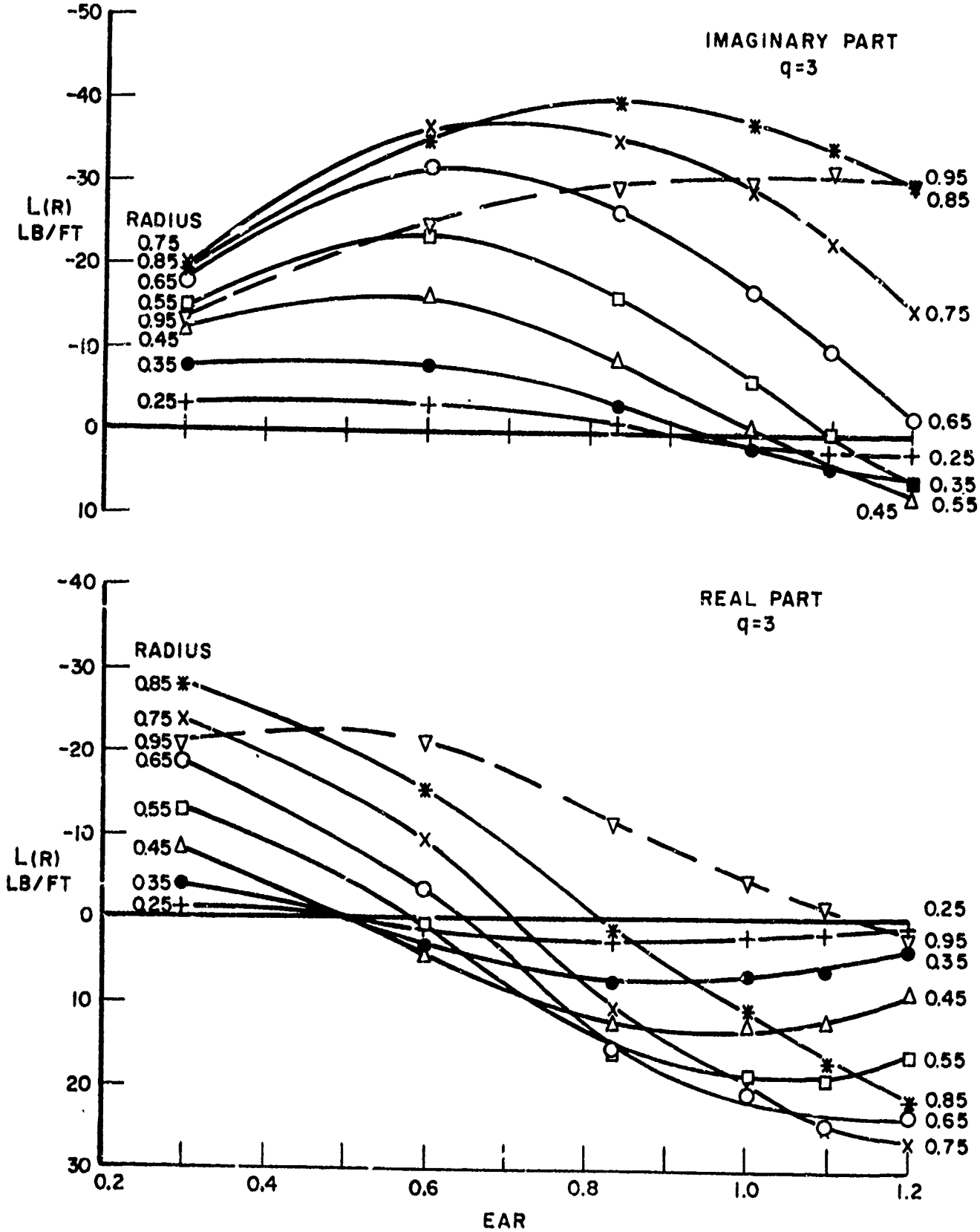

FIG. 4. SPANWISE LOADINGS VERSUS EAR FOR 3-BLADED PROPELLERS AT q=3

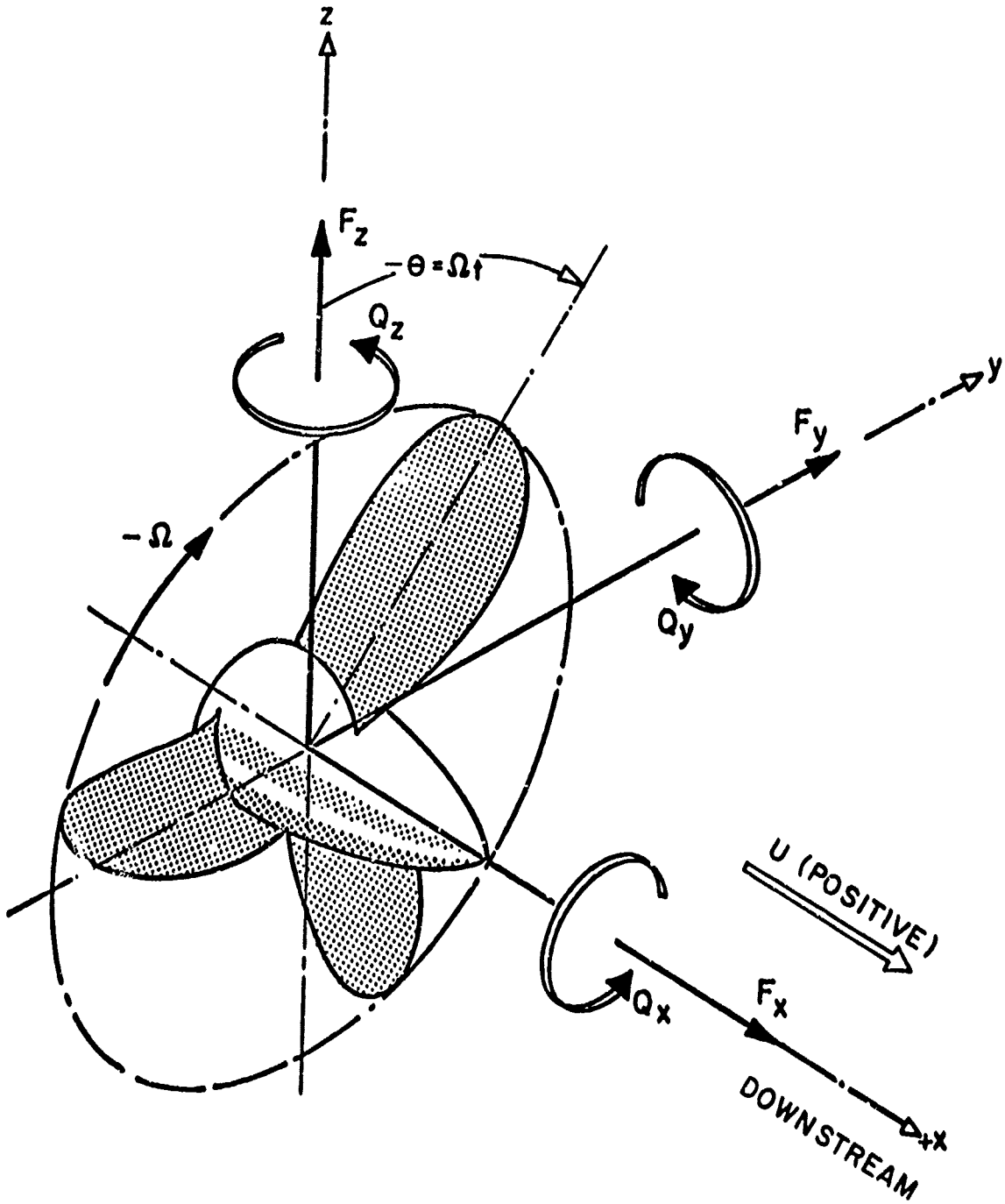

FIG. 5. RESOLUTION OF FORCES AND MOMENTS

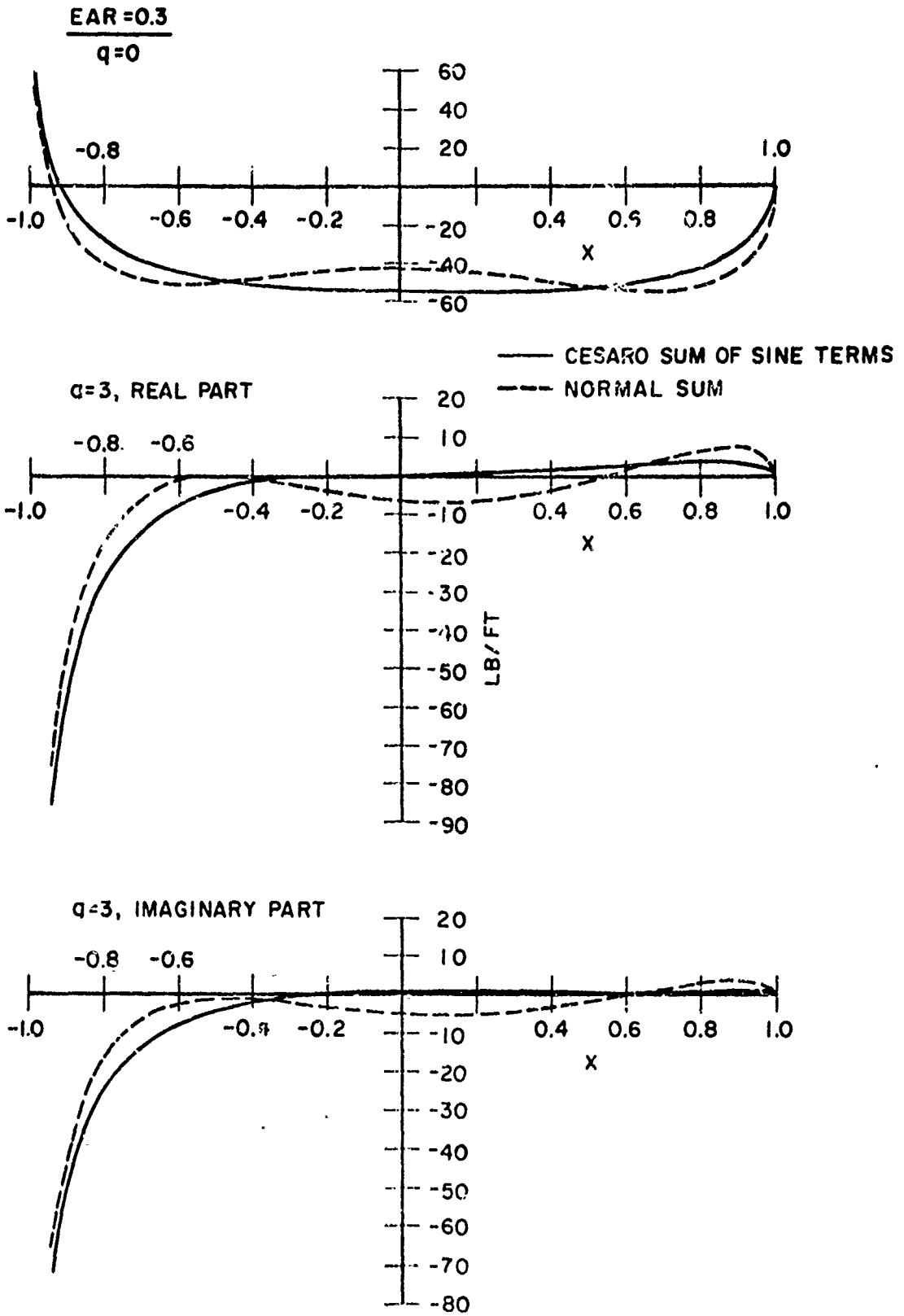

FIG. 6. CHORDWISE DISTRIBUTIONS AT 0.65 RADIUS FOR PROPELLER OF EAR = 0.3: COMPARISON OF NORMAL SUM AND CESARO SUM

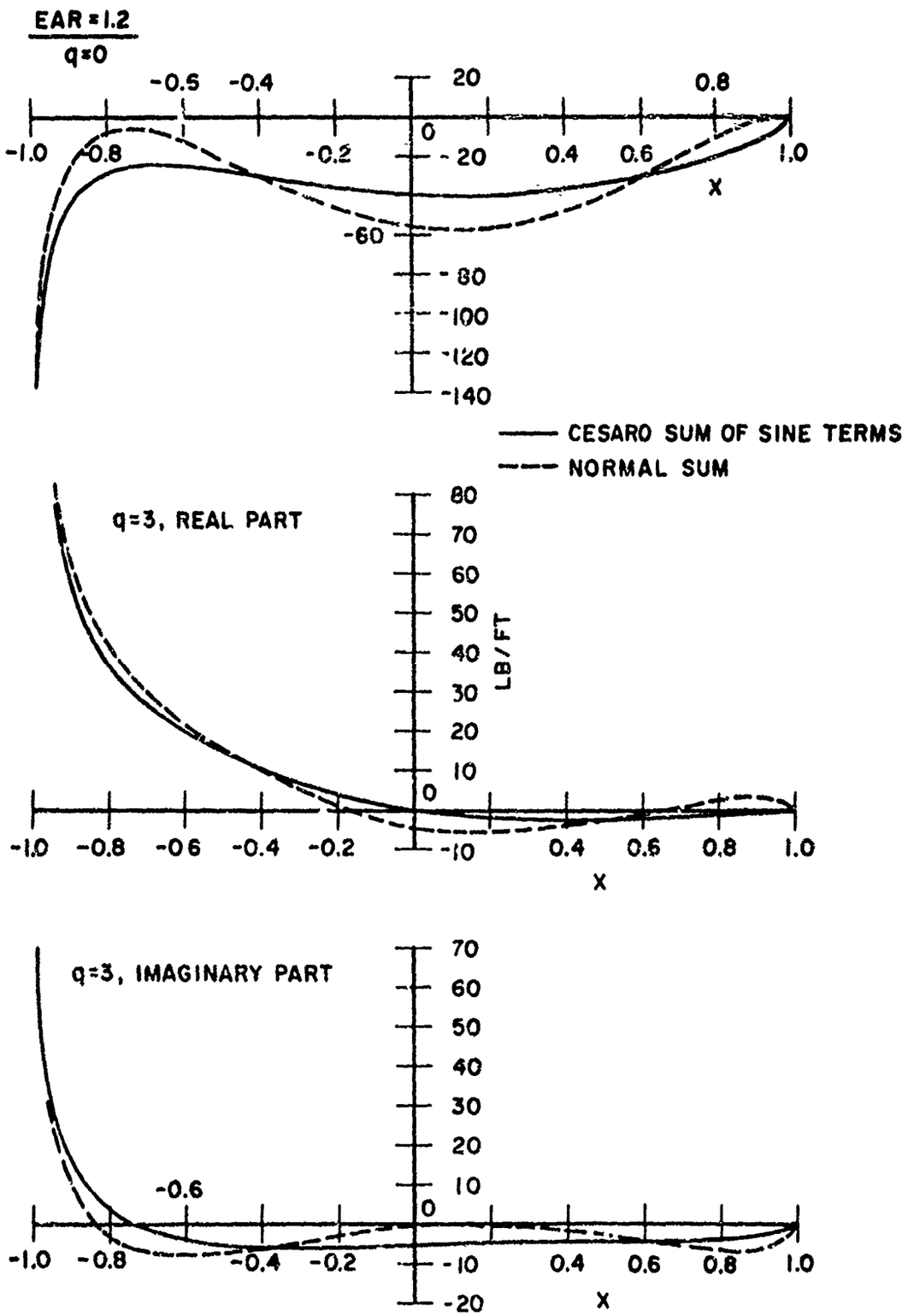

FIG. 7. CHORDWISE DISTRIBUTIONS AT 0.65 RADIUS FOR PROPELLER OF EAR = 1.2: COMPARISON OF NORMAL SUM AND CESARO SUM

Appendix A

Singularity of the Kernel Function at $\rho = r$

I Before the 1/K Expansion

If the substitution $\tau = \tau' - \xi$ is made in Equation (13), the kernel becomes

$$(4\pi\rho_f U)K = -\lim_{\delta\to 0} \sum_{n=1}^{N} e^{-iq\,\bar{\theta}_n} \frac{\partial}{\partial n'} \frac{\partial}{\partial n} \int_{-\infty}^{x-\xi} \frac{e^{iqa(\tau-x+\xi)}}{R}\, d\tau$$

$$\text{where } R = \left\{\tau^2 + r^2 + \rho^2 - 2r\rho \cos\left[\theta_o - \varphi_o + \bar{\theta}_n - a\,(\tau-x+\xi)\right]\right\}^{1/2} \qquad \text{(A-1)}$$

In the limit as $\delta\to 0$, R will go to zero when $\rho = r$, $\bar{\theta}_n = 0$, and $\tau = 0$. Therefore the singular behavior occurs when $n = 1$ and $x - \xi > 0$. For a study of this behavior, only that part of the τ-integration need be considered that is within a small range around $\tau = 0$, viz., $-\gamma \le \tau \le \gamma$ where γ is a sufficiently small but positive fixed number. Thus part of the kernel, for $n = 1$, may be designated by K_1

$$K_1 = -\lim_{\substack{\theta_o\to a\xi \\ \varphi_o\to ax}} \int_{-\gamma}^{\gamma} \frac{\partial}{\partial n'} \frac{\partial}{\partial n} \frac{e^{iqa(\tau-x+\xi)}}{R_1}\, d\tau \qquad \text{(A-2)}$$

After taking the derivatives and limits K_1 becomes

$$K_1 = -\frac{r\rho}{\sqrt{1 + a^2r^2}\sqrt{1 + a^2\rho^2}}\, e^{-iqa(x-\xi)} \int_{-\gamma}^{\gamma} e^{iqa\tau}$$

$$\cdot\left\{\frac{a^4q^2}{\sqrt{\tau^2 + r^2 + \rho^2 - 2r\rho \cos a\tau}} + \frac{ia^2q(2a^2r^2\rho^2 + r^2 + \rho^2)\sin a\tau}{r\rho(r^2 + r^2 + \rho^2 - 2r\rho\cos a\tau)^{3/2}}\right.$$

continued

$$+ \frac{(a^2\rho^2 + 1)\ (a^2r^2 + 1)\ \cos a\tau}{r\rho(\tau^2 + r^2 + \rho^2 - 2r\rho \cos a\tau)^{3/2}} - \frac{3(a^2\rho^2 + 1)\ (a^2r^2 + 1)\ \sin^2 a\tau}{(\tau^2 + r^2 + \rho^2 - 2r\rho \cos a\tau)^{5/2}}\ d\tau \Bigg\} \tag{A-3}$$

Let $\rho = r + \epsilon$ where ϵ is very small. Then the expressions involved in K_1 can be expanded in a series of ϵ and τ. After lengthy algebraic manipulation and trivial integrations, the singular behavior of K_1 is described by the following expression:

$$K_1 \approx - e^{-iqa(x-\xi)} \frac{r^2}{1 + a^2r^2} \left\{ \frac{2\sqrt{1 + a^2r^2}}{r^2(\rho - r)^2} + \frac{4a^2}{r\sqrt{1 + a^2r^2}} \frac{1}{\rho - r} \right\} \tag{A-4}$$

(as $\rho \to r$)

The first term has a high-order singularity with "Hadamard" finite contribution which is evaluated by the method of Mangler.[9] The second term is the well-known "Cauchy" type.

II After the 1/R Expansion

For the case of $n = 1$, $x-\xi > 0$, Eq (19) becomes after the limits have been taken

$$K_1 = - \frac{\rho r}{[(1+a^2\rho^2)(1+a^2r^2)]^{1/2}} \sum_{m=-\infty}^{\infty}$$

$$\Big\{ \left[a^2(m-q) + \frac{m}{r^2}\right] \left[a^2(m-q) + \frac{m}{\rho^2}\right] I_m(a\,|\,m-q\,|\,\rho) K_m(a\,|\,m-q\,|\,r)\, e^{-iaq(x-\xi)}$$

$$- \frac{i}{\pi} e^{-iam(x-\xi)} \int_{-\infty}^{\infty} \left(ak + \frac{m}{r^2}\right)\left(ak + \frac{m}{\rho^2}\right) e^{ik(x-\xi)} \frac{(IK)_m}{k - a(m-q)}\, dk \Big\} \tag{A-5}$$

where $(IK)_m = I_m(\,|\,k\,|\,\rho)\, K_m(\,|\,k\,|\,r)$

When $|m| \geq |M|$ large, the generalized mean-value theorem can be used for the integral term and this in conjunction with the residue theorem leads to

$$\int_c^d f(k)p(k)dk \approx f(A) \int_c^d p(k)d \qquad \begin{array}{l} c \leq A \leq d \\ p(k) \geq 0 \end{array}$$

with $p(k) = \dfrac{e^{ik(x-\xi)}}{k-a(m-q)}$

$$\int_{-\infty}^{\infty} f(k) \frac{e^{ik(x-\xi)}}{k-a(m-q)} dk \approx f(a(m-q)) \int_{-\infty}^{\infty} \frac{e^{ik(x-\xi)}}{k-a(m-q)} dk$$

$$\approx i\pi e^{ia(m-q)(x-\xi)} f(a(m-q)) \qquad \text{(A-6)}$$

$$\text{for } (x-\xi) > 0$$

Thus for large $|m|$ the integral term is approximately equal to the closed term and with $|m| \geq |M| \gg q$ K_1 reduces to

$$K_1 \approx -\frac{\rho r}{[(1+a^2\rho^2)(1+a^2r^2)]^{1/2}} \sum_{m=M}^{\infty} e^{-iaq(x-\xi)}$$

$$\cdot \left\{4 \frac{m^2}{r^2\rho^2} (1+a^2r^2)(1+a^2\rho^2) I_m(am\rho)\ K_m(amr)\right\} \qquad \text{(A-7)}$$

Nicholson[7] showed that the product $I_m(am\rho)K_m(amr)$ can be approximated by

$$I_m(am\rho)K_m(amr) \approx \frac{1}{[(1+a^2\rho^2)(1+a^2r^2)]^{1/4}} \frac{1}{2|m|} \left(\frac{\rho}{r}\right)^{|m|} \left(\frac{1+\sqrt{1+a^2r^2}}{1+\sqrt{1+a^2\rho^2}}\right)^{|m|}$$

$$\cdot e^{-|m|\left(\sqrt{1+a^2r^2} - \sqrt{1+a^2\rho^2}\right)} \qquad \text{(A-8)}$$

for $\rho < r$. (ρ and r are interchanged when $\rho > r$.)

If use is made of (A-8) then for m large, $m \gg q$

$$K_1 \approx -\frac{2}{r\rho} e^{-iaq(x-\xi)}[(1+a^2r^2)(1+a^2\rho^2)]^{1/4} \sum_{m=M}^{\infty} mX^m$$

$$\text{where} \quad X = \frac{\rho}{r}\left(\frac{1+\sqrt{1+a^2r^2}}{1+\sqrt{1+a^2\rho^2}}\right) e^{-(\sqrt{1+a^2r^2}-\sqrt{1+a^2\rho^2})}, \quad \rho < r \qquad \text{(A-9)}$$

It is known [8] that

$$\sum_{m=1}^{\infty} mX^m = \frac{X}{(1-X)^2} \quad \text{for} \quad X < 1$$

therefore

$$\sum_{m=M}^{\infty} mX^m = \frac{X}{(1-X)^2} - \sum_{m=1}^{M} mX^m$$

If only the terms of (A-9) giving rise to high-order singularities are considered (it is to be noted that the terms of (A-5) in q which were neglected give rise to a Cauchy type singularity), then

$$\lim_{\rho\to r} K_1 \approx \frac{-2e^{-iqa(x-\xi)}\sqrt{1+a^2r^2}}{r^2} \lim_{\rho\to r} \frac{X}{(1-X)^2}$$

$$\approx \frac{-2e^{-iqa(x-\xi)}\sqrt{1+a^2r^2}}{r^2} \frac{r^2}{1+a^2r^2} \lim_{\rho\to r} \frac{1}{(\rho-r)^2} \qquad \text{(A-10)}$$

since $\lim_{\rho\to r} \dfrac{\frac{X}{(1-X)^2}}{\frac{1}{(\rho-r)^2}}$ can be shown to be equal to $r^2/1+a^2r^2$

Equation (A-10) is identical with (A-4). Thus the expansion scheme for $1/R$ exhibits the proper singular behavior after the summation over m.

Appendix B

Evaluation of the θ_α- and φ_α-integrals

I. $$I^{(\bar{m})}(x) = \frac{1}{\pi} \int_0^\pi \Phi(\bar{m}) e^{ix\cos\varphi}\, d\varphi \qquad \text{(B-1)}$$

where for $\bar{m} = 1$

$$I^{(1)}(x) = \frac{1}{\pi} \int_0^\pi (1-\cos\varphi) e^{ix\cos\varphi}\, d\varphi = J_0(x) - iJ_1(x)$$

for $\bar{m} = 2$

$$I^{(2)}(x) = \frac{1}{\pi} \int_0^\pi (1+2\cos\varphi) e^{ix\cos\varphi}\, d\varphi = J_0(x) + i2J_1(x)$$

and for $\bar{m} > 2$

$$I^{(\bar{m})}(x) = \frac{1}{\pi} \int_0^\pi \cos(\bar{m}-1)\varphi\, e^{ix\cos\varphi} d\varphi = i^{\bar{m}-1} J_{\bar{m}-1}(x)$$

where $J_n(x)$ is the Bessel function of the first kind.

II. $$\Lambda^{(\bar{n})}(y) = \frac{1}{\pi} \int_0^\pi \Theta(\bar{n}) e^{-iy\cos\theta} \sin\theta d\theta \qquad \text{(B-2)}$$

For $\bar{n} = 1$

$$\Lambda^{(1)}(y) = \frac{1}{\pi} \int_0^\pi \cot\frac{\theta}{2} \sin\theta\, e^{-iy\cos\theta}\, d\theta = J_0(y) - iJ_1(y)$$

and for $\bar{n} > 1$

$$\Lambda^{(\bar{n})}(y) = \frac{1}{\pi} \int_0^\pi \sin(\bar{n}-1)\theta \sin\theta\, e^{-iy\cos\theta}\, d\theta$$

$$= \frac{(-i)^{\bar{n}-2}}{2} \left[J_{\bar{n}-2}(y) + J_{\bar{n}}(y) \right]$$

III. To evaluate the integrand of the λ-integral of Eq. (28) at the singularity $\lambda = 0$ (see Appendix C) it is necessary to define the following functions

$$\left.\frac{\partial I^{(\bar{m})}((q - \frac{\lambda}{a})\theta_b^r)}{\partial\lambda}\right|_{\lambda=0} = - i \frac{\theta_b^r}{a} I_1^{(\bar{m})}(q\theta_b^r) \tag{B-3}$$

and

$$\left.\frac{\partial\Lambda^{(\bar{n})}((q - \frac{\lambda}{a})\theta_b^\rho)}{\partial\lambda}\right|_{\lambda=0} = + i \frac{\theta_b^\rho}{a} \Lambda_1^{(\bar{n})}(q\theta_b^\rho) \tag{B-4}$$

where $I_1^{(\bar{m})}(2\theta_b^r) = \frac{1}{\pi}\int_0^\pi \Phi(\bar{m}) e^{iq\theta_b^r\cos\varphi} \cos\varphi \, d\varphi$

$$\Lambda_1^{(\bar{n})}(q\theta_b^\rho) = \frac{1}{\pi}\int_0^\pi \Theta(\bar{n}) \sin\theta\cos\theta \; e^{-iq\theta_b^\rho\cos\theta} \, d\theta$$

a) For $\bar{m} = 1$

$$I_1^{(1)}(x) = - 1/2 \left[J_o(x) - J_2(x)\right] + iJ_1(x)$$

for $\bar{m} = 2$

$$I_1^{(2)}(x) = \left[J_o(x) - J_2(x)\right] + iJ_1(x)$$

and for $\bar{m} > 2$

$$I_1^{(\bar{m})}(x) = \frac{i^{\bar{m}-2}}{2}\left[- J_{\bar{m}}(x) + J_{\bar{m}-2}(x)\right]$$

b) For $\bar{n} = 1$

$$\Lambda_1^{(1)}(y) = \frac{1}{2}\left[J_o(y) - J_2(y)\right] - iJ_1(y)$$

and for $\bar{n} > 1$

$$\Lambda_1^{(\bar{n})}(y) = \frac{(-i)^{\bar{n}+1}}{4}\left[J_{\bar{n}-3}(y) - J_{\bar{n}+1}(y)\right]$$

Appendix C

Evaluation of the Integrand of the λ-Integral (Equation 28) at the Singularity $\lambda = 0$

The integral of Eq. (28) is

$$\int_0^\infty \frac{g(\lambda) - g(-\lambda)}{\lambda} \tag{C-1}$$

where

$$g(\lambda) = I_m(i\lambda + a\ell N i\rho)\, K_m(i\lambda + a\ell N i r)\, B_{\bar{m},\bar{n}}(\lambda) e^{i\frac{\lambda}{a}\Delta\sigma} \quad \text{for } \rho \leq r$$

$$B_{\bar{m},\bar{n}}(\lambda) = \left(a\lambda + a^2\ell N + \frac{m}{r^2}\right)\left(a\lambda + a^2\ell N + \frac{m}{\rho^2}\right) I^{(\bar{m})}\left(\left(q - \frac{\lambda}{a}\right)\theta_b^r\right) \Lambda^{(\bar{n})}\left(\left(q - \frac{\lambda}{a}\right)\theta_b^\rho\right)$$

$$m = q + \ell N$$

By L'Hospital's rule the integrand at $\lambda = 0$ becomes

$$\lim_{\lambda \to 0} \frac{g(\lambda) - g(-\lambda)}{\lambda} = \left[\frac{\partial g(\lambda)}{\partial \lambda} - \frac{\partial g(-\lambda)}{\partial \lambda}\right]_{\lambda=0} \tag{C-2}$$

It is obvious that

$$B_{\bar{m},n}(\lambda)\Big|_{\lambda=0} = B_{\bar{m},\bar{n}}(-\lambda)\Big|_{\lambda=0}$$

$$\left[I_m(i\lambda + a\ell N i\rho) K_m(i\lambda + a\ell N i r)\right]_{\lambda=0} = \left[I_m(i-\lambda + a\ell N i\rho) K_m(i-\lambda + a\ell N i r)\right]_{\lambda=0}$$

and $$e^{i\frac{\lambda}{a}\Delta\sigma}\Big|_{\lambda=0} = e^{-i\frac{\lambda}{a}\Delta\sigma}\Big|_{\lambda=0}$$

Then

$$\left[\frac{\partial g(\lambda)}{\partial\lambda} - \frac{\partial g(-\lambda)}{\partial\lambda}\right]_{\lambda=0} = 2i\,\frac{\Delta\sigma}{a}\,(IK)_m\Big|_{\lambda=0} B_{\bar{m},\bar{n}}(0)$$

$$+ (IK)_m\Big|_{\lambda=0}\left[\frac{\partial B_{\bar{m},\bar{n}}(\lambda)}{\partial\lambda} - \frac{\partial B_{\bar{m},\bar{n}}(-\lambda)}{\partial\lambda}\right]_{\lambda=0}$$

$$+ B_{\bar{m},\bar{n}}(0)\left\{\frac{\partial\left[I_m(I\lambda+a\ell NI\rho)K_m(I\lambda+a\ell NIr)\right]}{\partial\lambda}\right.$$

$$\left. - \frac{\partial\left[I_m(I-\lambda+a\ell NI\rho)K_m(I-\lambda+a\ell NIr)\right]}{\partial\lambda}\right\}_{\lambda=0} \qquad \text{(C-3)}$$

Here $(IK)_m\Big|_{\lambda=0} = I_m(Ia\ell NI\rho)K_m(Ia\ell NIr)$ for $\rho \le r$ (C-4)

$$\frac{-\partial B_{\bar{m},\bar{n}}(-\lambda)}{\partial\lambda}\Big|_{\lambda=0} = \frac{+\partial B_{\bar{m},\bar{n}}(\lambda)}{\partial\lambda}\Big|_{\lambda=0} = a\left(2a^2\ell N + \frac{m}{r^2} + \frac{m}{\rho^2}\right) I^{(\bar{m})}(q\theta_b^r)\Lambda^{(\bar{n})}(q\theta_b^\rho)$$

$$+ \frac{i}{a}\left(a^2\ell N + \frac{m}{r^2}\right)\left(a^2\ell N + \frac{m}{\rho^2}\right)\left[-\theta_b^r I_1^{(\bar{m})}(q\theta_b^r)\Lambda^{(\bar{n})}(q\theta_b^\rho) + \theta_b^\rho I^{(\bar{m})}(q\theta_b^r)\Lambda_1^{(\bar{n})}(q\theta_b^\rho)\right]$$

(C-5)

and $I_1^{(\bar{m})}(x)$ and $\Lambda_1^{(\bar{n})}(x)$ are as defined in Appendix B.

The third term of (C-3) is treated as follows:

a) For $\lambda = 0+$ and $a\ell N > 0$

$$I_m(I\lambda+a\ell NI\rho)K_m(I\lambda+a\ell NIr) = I_m((\lambda+a\ell N)\rho)K_m((\lambda+a\ell N)r)$$

and

$$I_m(I-\lambda+a\ell NI\rho)K_m(I-\lambda+a\ell NIr) = I_m((a\ell N-\lambda)\rho)K_m((a\ell N-\lambda)r)$$

so that the third term of (C-3) becomes

$$2B_{\bar{m},\bar{n}}(0)\,\frac{\partial\left[I_m((\lambda+Ia\ell NI)\rho)K_m((\lambda+Ia\ell NI)r)\right]}{\partial\lambda}\Big|_{\lambda=0} \quad (\text{for } \rho \le r)$$

$$= 2B_{\bar{m},\bar{n}}(0)\left\{\frac{\rho}{2} K_m(|a\ell N|r)\left[I_{m-1}(|a\ell N|\rho) + I_{m+1}(|a\ell N|\rho)\right]\right.$$

$$\left. - \frac{r}{2} I_m(|a\ell N|\rho)\left[K_{m-1}(|a\ell N|r) + K_{m+1}(|a\ell N|r)\right]\right. \qquad \text{(C-6)}$$

(Note that for $\rho \geq r$, ρ and r are interchanged in Eqs. C-3, C-4 and C-6.)

b) For $\lambda = 0+$ and $a\ell N < 0$

$$I_m(|\lambda+a\ell N|\rho)K_m(|\lambda+a\ell N|r) = I_m((|a\ell N|-\lambda)\rho)K_m((|a\ell N|-\lambda)r)$$

and

$$I_m(|-\lambda+a\ell N|\rho)K_m(|-\lambda+a\ell N|r) = I_m((|a\ell N|+\lambda)\rho)K_m((|a\ell N|+\lambda)r)$$

The third term of C-3 then becomes

$$- 2B_{\bar{m},\bar{n}}(0) \left.\frac{\partial\left[I_m((\lambda+|a\ell N|)\rho)K_m((\lambda+|a\ell N|)r)\right]}{\partial\lambda}\right|_{\lambda=0} \text{ for } \rho \leq r \qquad \text{(C-7)}$$

Therefore Eq. (C-3) can be written as

$$\left[\frac{\partial g(\lambda) - \partial(g-\lambda)}{\partial\lambda}\right]_{\lambda=0} = 2i\,\frac{\Delta\sigma}{a}\,(IK)_m\Big|_{\lambda=0} B_{\bar{m},\bar{n}}(0)$$

$$+ 2(IK)_m\Big|_{\lambda=0} \left.\frac{\partial B_{\bar{m},\bar{n}}(\lambda)}{\partial\lambda}\right|_{\lambda=0} \pm 2B_{\bar{m},\bar{n}}(0) \left.\frac{\partial(IK)_m}{\partial\lambda}\right|_{\lambda=0} \qquad \text{(C-8)}$$

where $(IK)_m\Big|_{\lambda=0}$ is given in (C-4)

$$B_{\bar{m},\bar{n}}(0) = \left(a^2\ell N + \frac{m}{r^2}\right)\left(a^2\ell N + \frac{m}{\rho^2}\right) I^{(\bar{m})}(q\theta_b^r)\Lambda^{(\bar{n})}(q\theta_b^\rho)$$

$$\left.\frac{\partial B_{\bar{m},\bar{n}}(\lambda)}{\partial\lambda}\right|_{\lambda=0} \text{ is given in (C-5)}$$

$$\left.\frac{\partial(IK)_m}{\partial\lambda}\right|_{\lambda=0} \text{ is given in (C-6)}$$

and the upper sign is taken when $\ell > 0$ and the lower sign when $\ell < 0$.

When $\ell = m = q = 0$, by the limiting process, it is easily shown that

$$\lim_{\ell\to 0} B_{\bar{m},\bar{n}}(0) \to \lim_{\ell\to 0} \ell^2 \to 0$$

$$\lim_{\ell\to 0} B_{\bar{m},\bar{n}}(0) \left.\frac{\partial (IK)_o}{\partial\lambda}\right|_{\lambda=0} \to \lim_{\ell\to 0} \frac{\ell^2}{\ell} \to 0$$

$$\lim_{\ell\to 0} \left.(IK)_o\right|_{\lambda=0} \cdot B_{\bar{m},\bar{n}}(0) \to \lim_{\ell\to 0} \ell^2 \log\ell \to 0$$

$$\lim_{\ell\to 0} \left.(IK)_o\right|_{\lambda=0} \left.\frac{\partial B_{\bar{m},\bar{n}}(\lambda)}{\partial\lambda}\right|_{\lambda=0} \to \lim_{\ell\to 0} (\ell+\ell^2)\log\ell \to 0$$

Hence when $\ell = m = q = 0$

$$\lim_{\lambda\to 0} \frac{g(\lambda) - g(-\lambda)}{\lambda} \to 0 \tag{C-9}$$

When $\ell = 0$ but $m = q \neq 0$, it is easily shown that

$$\lim_{\ell\to 0} \left.(IK)_m\right|_{\lambda=0} = \begin{cases} \frac{1}{2|m|} \left(\frac{\rho}{r}\right)^{|m|} & \text{for } \rho \le r \\ \frac{1}{2|m|} \left(\frac{r}{\rho}\right)^{|m|} & \text{for } \rho \ge r \end{cases}$$

$$\lim_{\ell\to 0} \left.\frac{\partial (IK)_m}{\partial\lambda}\right|_{\lambda=0} \to 0$$

Hence for $\ell = 0$, $m = q \neq 0$

$$\begin{aligned} \lim_{\lambda\to 0} \frac{g(\lambda)-g(-\lambda)}{\lambda} \to 2 & \left\{ \lim_{\ell\to 0} \left.(IK)_m\right|_{\lambda=0} \right\} \\ & \cdot \left\{ I^{(\bar{m})}(q\theta_b^r)\Lambda^{(\bar{n})}(q\theta_b^\rho)\left[I \frac{\Delta\sigma}{a} \frac{m^2}{r^2\rho^2} + am\left(\frac{1}{r^2} + \frac{1}{\rho^2}\right)\right] \right. \\ & \left. - \frac{im^2}{ar^2\rho^2}\left[\theta_b^r I_1^{(\bar{m})}(q\theta_b^r)\Lambda^{(\bar{n})}(q\theta_b^\rho) - \theta_b^\rho I^{(\bar{m})}(q\theta_b^r)\Lambda_1^{(\bar{n})}(q\theta_b^\rho)\right] \right\} \end{aligned} \tag{C-10}$$

When $q = 0$ and Eq. (36b) is used for the kernel functions, the value of the integrand at $\lambda = 0$ is zero for $m = 0$. For $m \pm 0$ it can be easily shown that the integrand at $\lambda = 0$ when $q = 0$, $\dot{m} = \ell N$ is

$$i\,\frac{4m^2}{a}\left(a^2+\frac{1}{r^2}\right)\left(a^2+\frac{1}{\rho^2}\right) I_m(am\rho)K_m(amr)$$

$$\cdot\left\{\Delta\sigma I^{(\bar{m})}(0)\Lambda^{(\bar{n})}(0) - \theta_b^r\, I_1^{(\bar{m})}(0)\Lambda^{(\bar{n})}(0) + \theta_b^\rho\, I^{(\bar{m})}(0)\Lambda_1^{(\bar{n})}(0)\right\} \quad \text{(C-11)}$$

Appendix D

Evaluation by the Lagrange Interpolation Method of the ρ-Integration in the Region of the Singularity

The ρ-integration of the kernel function in the region of the singularity is in the form

$$I = \int_{r-\beta}^{r+\beta} \frac{M(r,\rho;q)}{(\rho-r)^3}\, d\rho \tag{D-1}$$

where $M(r,\rho;q) = (\rho-r)^3\, K^{(\bar{m},\bar{n})}(r,\rho;q)$.

Since $K^{(\bar{m},\bar{n})}$ varies as $(\rho-r)^{-2}$ as $\rho \to r$, $M = 0$ when $\rho = r$. For this reason the function M can easily be expanded about the singularity $\rho = r$ by the Lagrange formula

$$M(\rho) = \sum_{i=0}^{n} \frac{\Pi_n(\rho)}{(\rho - \rho_i)\, \Pi_n'(\rho_i)} M_{i+1} \qquad i = 0, 1, \ldots n$$

where

$$\Pi_n(\rho) = (\rho - \rho_o)\,(\rho - \rho_1)\, \ldots\, (\rho - \rho_n)$$

$$\Pi_n'(\rho_i) = \frac{d}{d\rho}\, \Pi_n(\rho) \text{ evaluated at } \rho = \rho_i \tag{D-2}$$

and $M_{i+1} = M(\rho_i)$ (see Scarborough[11] and Watkins et al[12]).

In the strip from $r - \beta$ to $r + \beta$ (with $n = 4$ for the 5-point formula), $\rho_o = r - \beta = r - 2\delta$, $\rho_1 = r - \delta$, etc. where $\delta = \beta/2$. Then

$$\Pi_n'(\rho_i) = (-1)^{4-i}\, \delta^4\, i!\, (4-i)!$$

and

$$M(\rho) = \frac{1}{\delta^4} \sum_{i=0}^{4} \frac{(-1)^i}{i!\,(4-i)!} \frac{(\rho-r+2\delta)(\rho-r+\delta)(\rho-r)(\rho-r-\delta)(\rho-r-2\delta)}{\rho - r + (2-i)\delta} M_{i+1}$$

where $M_3 = 0$ since $\rho_2 = r$. (D-3)

The integral I is

$$I = \int_{r-2\delta}^{r+2\delta} \frac{M(\rho)}{(\rho-r)^3}\, d\rho = \frac{1}{\delta^4} \int_{r-2\delta}^{r+2\delta} [g_o(\rho-r) + \delta g_1] d\rho$$

$$+ \frac{g_2}{\delta^2} \int_{r-2\delta}^{r+2\delta} \frac{d\rho}{\rho-r} + \frac{g_3}{\delta} \int_{r-2\delta}^{r+2\delta} \frac{d\rho}{(\rho-r)^2} \qquad \text{(D-4)}$$

where

$$g_o = \frac{M_1 + M_5}{4!} - \frac{M_2 + M_4}{3!}$$

$$g_1 = \frac{2(M_5 - M_1)}{4!} - \frac{(M_4 - M_2)}{3!}$$

$$g_2 = \frac{-(M_1 + M_5)}{4!} + \frac{4(M_2 + M_4)}{3!}$$

$$g_3 = \frac{2(M_1 - M_5)}{4!} - \frac{4(M_2 - M_4)}{3!}$$

The Cauchy principal value is to be taken of the second integral:

$$\oint_{r-2\delta}^{r+2\delta} \frac{d\rho}{\rho-r} = 0$$

The last integral is the Hadamard type whose finite contribution is

$$\int_{r-2\delta}^{r+2\delta} \frac{d\rho}{(\rho-r)^2} = \lim_{\epsilon\to 0} \left[\int_{r-2\delta}^{r-\epsilon} + \int_{r+\epsilon}^{r+2\delta} + \int_{r-\epsilon}^{r+\epsilon}\right] \frac{d\rho}{(\rho-r)^2}$$

$$= \lim_{\epsilon\to 0} \left[-\frac{1}{\rho-r}\right]_{r-2\delta,\ r+\epsilon,\ r-\epsilon}^{r-\epsilon,\ r+2\delta,\ r+\epsilon}$$

$$= -\frac{1}{\delta}$$

Therefore

$$I = \frac{1}{\delta^4}\left[\delta g_1 \cdot \rho\right]_{r-2\delta}^{r+2\delta} - \frac{g_3}{\delta^2}\Big]$$

$$= \frac{1}{\delta^4}\left[4\delta^2 g_1\right] - \frac{g_3}{\delta^2} = \frac{1}{\delta^2}\,(4g_1 - g_3)$$

or

$$I = \frac{1}{\delta^2}\left[\frac{5}{12}\,(M_5 - M_1) - \frac{4}{3}(M_4 - M_2)\right] \qquad \text{(D-5)}$$

where

$$M_1 = -8\delta^3 \cdot K^{(\bar{m},\bar{n})}(\rho = r - 2\delta)$$

$$M_2 = -\delta^3 \cdot K^{(\bar{m},\bar{n})}(\rho = r - \delta)$$

$$M_4 = \delta^3 \cdot K^{(\bar{m},\bar{n})}(\rho = r + \delta)$$

$$M_5 = 8\delta^3 \cdot K^{(\bar{m},\bar{n})}(\rho = r + 2\delta)$$

and

$$\delta = \beta/2$$